Clim. Past, 18, 1797–1813, 2022
https://doi.org/10.5194/cp-18-1797-2022

Climate of the Past
Open Access
EGU

Bottom water oxygenation changes in the southwestern Indian Ocean as an indicator for enhanced respired carbon storage since the last glacial inception

Helen Eri Amsler[1,2], Lena Mareike Thöle[1,2,3], Ingrid Stimac[4], Walter Geibert[4], Minoru Ikehara[5], Gerhard Kuhn[4], Oliver Esper[4], and Samuel Laurent Jaccard[1,2,6]

[1]Institute of Geological Sciences, University of Bern, Bern, Switzerland
[2]Oeschger Centre for Climate Change Research, University of Bern, Bern, Switzerland
[3]Department of Earth Sciences, Utrecht University, Utrecht, the Netherlands
[4]Alfred-Wegener-Institut Helmholtz-Zentrum für Polar- und Meeresforschung, Bremerhaven, Germany
[5]Center for Advanced Marine Core Research, Kochi University, Kochi, Japan
[6]Institute of Earth Sciences, University of Lausanne, Lausanne, Switzerland

Correspondence: Helen Eri Amsler (eri.amsler@unibe.ch) and Samuel L. Jaccard (samuel.jaccard@unil.ch)

Received: 15 March 2021 – Discussion started: 20 April 2021
Revised: 29 April 2022 – Accepted: 1 June 2022 – Published: 9 August 2022

Abstract. We present downcore records of redox-sensitive authigenic uranium (U) and manganese (Mn) concentrations based on five marine sediment cores spanning a meridional transect encompassing the Subantarctic and Antarctic zones in the southwestern Indian Ocean covering the last glacial cycle. These records signal lower bottom water oxygenation during glacial climate intervals and generally higher oxygenation during warm periods, consistent with climate-related changes in deep-ocean remineralized carbon storage. Regional changes in the export of siliceous phytoplankton to the deep sea may have entailed a secondary influence on oxygen levels at the water–sediment interface, especially in the Subantarctic Zone. The rapid reoxygenation during the deglaciation is in line with increased ventilation and enhanced upwelling after the Last Glacial Maximum (LGM), which in combination conspired to transfer previously sequestered remineralized carbon to the surface ocean and the atmosphere, contributing to propel the Earth's climate out of the last ice age. These records highlight the still insufficiently documented role that the Southern Indian Ocean played in the air–sea partitioning of CO_2 on glacial–interglacial timescales.

1 Introduction

On glacial–interglacial timescales, the ocean plays a dominant role in regulating changes in the global carbon cycle (e.g., Sigman and Boyle, 2000), as the deep ocean has a sufficiently voluminous and dynamic carbon reservoir to modulate the air–sea partitioning of CO_2 and by inference climate. In particular, the Southern Ocean acts as a major conduit connecting the vast ocean interior and the atmosphere, as deep CO_2-rich water masses outcrop along tilted density surfaces (isopycnals) promoting exchange with the atmosphere (Marshall and Speer, 2012; Talley, 2013).

Accordingly, a number of distinct and often synergistic mechanisms, focusing on changes in Southern Ocean circulation, nutrient biogeochemistry, and sea ice dynamics have been proposed to have contributed to lower atmospheric CO_2 during past ice ages (e.g., Adkins, 2013; Ferrari et al., 2014; Hain et al., 2010; Sigman et al., 2010, 2021). However, the mechanisms accounting for the generally reduced glacial atmospheric CO_2 inventory are still debated and not yet fully resolved. Radiocarbon (^{14}C) data suggest that the deep (> 1000–1500 m) ocean was generally more poorly ventilated during the last ice age than during the Holocene (Sarnthein et al., 2013; Skinner et al., 2017) (although a portion of this signal could be related to decreased air–sea gas exchange; Galbraith et al., 2015). The formation of saltier (less

buoyant) bottom waters around Antarctica due to more dynamic sea ice cycling would have strengthened the vertical stratification and isolation of deeper waters during the Last Glacial Maximum (LGM) (Adkins, 2013; Adkins et al., 2002; Bouttes et al., 2010; Ferrari et al., 2014; Stein et al., 2020). Furthermore, a northward shift of the upwelling region might have led to the exposure of shallower waters, resulting in reduced CO_2 outgassing and enhanced carbon sequestration in the ocean interior (Sigman and Boyle, 2000; Toggweiler, 1999; Toggweiler et al., 2006; Watson et al., 2015).

In addition to these physical mechanisms affecting ocean circulation, changes in marine biology and nutrient biogeochemistry further contributed to sequester carbon away from the atmosphere (Francois et al., 1997; Galbraith and Jaccard, 2015; Sigman and Boyle, 2000; Sigman et al., 2010, 2021). A generally more efficient biological carbon pump during glacial periods, sustained by generally more complete nutrient utilization and/or increased Fe-bearing dust supply would have contributed to curb CO_2 outgassing from the Southern Ocean (e.g., Ai et al., 2020; Galbraith and Skinner, 2020; Gottschalk et al., 2016; Jaccard et al., 2013; Kohfeld et al., 2005; Kumar et al., 1995; Martínez-García et al., 2014; Sigman et al., 2010; Studer et al., 2015).

At the onset of the last glacial termination (TERM I) approximately 17.5 ka ago, Southern Ocean ventilation resumed as the Earth emerged from the last ice age, and previously sequestered, radiocarbon-depleted CO_2 was released to the atmosphere (e.g., Basak et al., 2018; Bauska et al., 2016; Burke and Robinson, 2012; Gottschalk et al., 2016, 2020b; Jaccard et al., 2016; Rae et al., 2018; Skinner et al., 2010). Coupled with enhanced upwelling, nutrient- and CO_2-rich subsurface waters were transported to the sunlit surface ocean, supporting high levels of biological production with less complete nutrient consumption south of the Polar Front (e.g., Anderson et al., 2009; Frank et al., 2000; Jaccard et al., 2013; Kohfeld et al., 2005; Thöle et al., 2019). At the same time, the Fe-bearing dust supply started to dwindle, causing biogenic export production to decline in the Subantarctic Zone of the Southern Ocean (Anderson et al., 2014; Jaccard et al., 2016, 2013; Martínez-García et al., 2014; Thöle et al., 2019), further decreasing marine carbon storage. In combination, these processes would thus have contributed to increase atmospheric CO_2 concentrations, providing the necessary impetus for Earth's climate to transition out of the last ice age.

While this narrative represents the prevailing regionally integrated understanding of the leverage the Southern Ocean bears on the air–sea partitioning of CO_2 across the last deglacial termination, observations are largely based on records from the southern Atlantic. Records from the Pacific and Indian sectors of the Southern Ocean are consistent with the first-order paleoceanographic evolution described above, but regional specificities exist. In particular, it remains unclear how export production patterns vary regionally in the Indian sector of the Southern Ocean characterized by a complex frontal structure (e.g., Durgadoo et al., 2008). Additionally, the source of bioavailable Fe, which is crucial to sustain phytoplankton growth, may vary regionally. Indeed, observations suggest that a large fraction of the Fe supplied to the open Indian Ocean may arise from deep winter mixing (Tagliabue et al., 2014).

Reconstructing past changes in bottom water oxygenation has the potential to further disentangle and offer a clearer understanding of some of these processes. Variations in the storage of respiratory carbon are accompanied by large changes in dissolved oxygen concentration associated with organic matter remineralization (e.g., Anderson et al., 2019; Gottschalk et al., 2016, 2020b; Hoogakker et al., 2015; Jaccard et al., 2016; Jacobel et al., 2017). The temporal evolution of bottom water oxygenation can thus be reconstructed qualitatively using the distribution of redox-sensitive metals in the marine sedimentary record (e.g., Calvert and Pedersen, 1996; Francois et al., 1997; Frank et al., 2000; Nameroff et al., 2002). Here, we focus on authigenic uranium (U) and manganese (Mn), which are both sensitive to dissolved oxygen concentrations typically encountered in open-ocean conditions. The analyses were carried out on a set of five marine sediment cores spanning a meridional transect in the still underrepresented Indian sector of the Southern Ocean. Combining these observations with preserved opal flux reconstructions allows for deciphering the different processes affecting bottom water oxygenation and inferring their relative contributions in sequestering CO_2 in the ocean interior, away from the atmosphere. The core site locations were characterized by temporally contrasted export production patterns (Manoj and Thamban, 2015; Nair et al., 2019) and thus provide an interesting case study to critically test some of the prevailing assumptions underlying the sequence of events, which lead the Earth's climate to transition into the last ice age.

2 Study site, materials, and methods

2.1 Core locations and material

The five marine sediment cores were retrieved along a meridional transect including Del Caño Rise and Conrad Rise and reaching as far south as Enderby Abyssal Plain in the SW Indian Ocean (Fig. 1). Cores DCR-1PC (46°01.34′ S, 44°15.24′ E, 2632 m b.s.l.) and COR-1bPC (54°16.04′ S, 39°45.98′ E, 2828 m b.s.l.) were collected during expedition KH-10-7 on R/V *Hakuho-maru* in 2010–2011. The sediment cores were retrieved from the southern flank of Del Caño Rise (DCR-1PC) and Conrad Rise (COR-1bPC), respectively. Cores PS2609-1 (51°29.9′ S, 41°35.8′ E, 3113 m b.s.l.), PS2606-6 (53°13.9′ S, 40°48.1′ E, 2545 m b.s.l.), and PS2603-3 (58°59.2′4 S, 37°37.7′ E, 5289 m b.s.l.) were retrieved during ANT-XI/4 expedition on R/V *Polarstern* in 1994. Cores PS2609-1 and PS2606-6 were retrieved from Conrad Rise as well: the former on its north-

ern flank and the latter on the rise itself. Core PS2603-3 is located furthest to the south in the Enderby Abyssal Plain and at the greatest water depth of the five cores. All cores are bathed by Circumpolar Deep Water (CDW) with the exception of core PS2603-3, which is influenced by Antarctic Bottom Water (AAWB) (Fig. 1). CDW comprises variable contributions of North Atlantic Deep Water (NADW), as well as recirculated deep water originating from the Pacific and Indian Ocean basins. CDW is typically depleted in dissolved oxygen as the water mass is not ventilated at the ocean surface but instead forms as a blend of pre-aged subsurface water masses.

DCR-1PC is the northernmost core and lies in the Subantarctic Zone (SAZ) of the Southern Ocean; it is composed of nannofossil and diatom ooze with variable amounts of clay. All other cores predominantly consist of diatom ooze (Kuhn, 2003a, b, c; Oiwane et al., 2014) with variable amounts of lithogenic material and lie south of today's position of the Polar Front (PF) in the Antarctic Zone (AZ).

2.2 Age models

For DCR-1PC, seven radiocarbon (^{14}C) ages were obtained using mono-specific samples of planktic foraminifera *Globigerina bulloides* and *Neogloboquadrina pachyderma* (sinistral) using the accelerator mass spectrometry (AMS) facilities at the University of Tokyo (Crosta et al., 2020). Calibration of the ^{14}C measurements was performed using the CALIB7.02 software and the Marine13 calibration curve (Reimer et al., 2013) applying a regionally informed marine reservoir age correction of 890 ± 100 years (Butzin et al., 2005). The Marine13 calibration curve was given preference because the Marine20 curve is not adequate for application in polar regions characterized by variable sea ice extent (Heaton et al., 2020). In addition to the ^{14}C dates, the diatom-based sea surface temperature (SST) record was graphically aligned to the EPICA Dome C deuterium (δD) record, assuming both records are synchronous (Crosta et al., 2020). It is worth noting that the depth interval 33–41 cm is characterized by a substantial reduction in sedimentation accumulation rates, possibly reminiscent of a sedimentary hiatus (Fig. 2).

The stratigraphy for core COR-1bPC is based on 23 calibrated ^{14}C measurements using mono-specific samples of planktic foraminifera *Neogloboquadrina pachyderma* (sinistral) (Oiwane et al., 2014). All dates were corrected for the regional reservoir age (890 years) (Bard, 1988) and converted to calibrated years before present (cal yr BP) using the CALIB 6.1.0 software package (Stuiver and Reimer, 1993).

Regarding the PS cores, preliminary age pointers were based on available radiocarbon dates (Xiao et al., 2016) and biostratigraphic constraints (Table 1). The ^{14}C measurements were obtained via AMS using the sedimentary humic acid fraction in the absence of sufficiently well-preserved foraminiferal carbonate. Radiocarbon ages were calibrated using the CALIB4.2 (Stuiver et al., 1998) software package after applying a reservoir age correction of 810 years (Bard, 1988). The preliminary age models were first refined by graphically aligning biogenic opal ($BSiO_2$) measurements to the LR04 δ^{18}O benthic stack, assuming an in-phase relationship. This approach inherently assumes that sedimentary $BSiO_2$ concentrations are modulated by climate variability in the Southern Ocean (e.g., Hasenfratz et al., 2019) and more specifically in the Indian sector of the Southern Ocean (Kaiser et al., 2021; Manoj and Thamban, 2015). Similarly, the sedimentary magnetic susceptibility (MagSus) signal contains a coherent climate-related component and was thus used for initial age model tuning of cores PS2609-1 and PS2606-6 (e.g., Weber et al., 2012, 2014). These age solutions were then further refined by graphically aligning the X-ray fluorescence (XRF) Ca / Ti and Ti records to the EPICA Dome C (EDC) dust record (Lambert et al., 2012) for cores PS2609-1 and PS2606-6 (Table 1) and assuming an in-phase relationship between both proxies and archives (e.g., Martínez-Garcia et al., 2014; Lamy et al., 2014). For the age model for core PS2603-3, the extinctions of three diatom species served as additional biostratigraphic markers (Table 1): *Rouxia leventerae* at 130 ka, *Hemidiscus karstenii* at 191 ka, and *Rouxia constricta* at 300 ka (Zielinski and Gersonde, 2002). There is evidence for a 30 kyr sedimentary hiatus associated with a sediment disturbance at the marine isotope stage (MIS) 5–MIS 4 boundary. Independent absolute age constraints with the constant rate supply (CRS) model (Geibert et al., 2019) yielded similar ages for PS2603-3, except for the interval around the hiatus. Finally, the age models have been tested by comparing the solutions to independently defined age models. Specifically, our age model for PS2606-6 is very similar to the stratigraphic framework published by Ronge et al. (2020). The age model for core PS2603-3, which arguably contains the fewest tie points, was critically assessed using an independent approach based on CRS (Geibert et al., 2019). Both approaches provided very similar ages, with age offsets of < 1.5 kyr for the last 20 kyr. In summary, the presented age models may certainly be perfectible, but given the constraints and limitations they are probably realistic and permit meaningful regional comparisons on multi-millennial timescales.

2.3 Bottom water oxygenation proxies

In oxygenated seawater, uranium (U) is present as soluble U(VI). In oxygen-depleted environments, however, U is reduced and precipitated as insoluble U(IV) in the form of uraninite (Langmuir, 1978; Morford and Emerson, 1999). Uranium concentrations in sediment porewaters decreases under reducing conditions, creating a concentration gradient between bottom waters and the uppermost sediment layers. This gradient leads to the diffusion of dissolved U into the sediment and to the precipitation of authigenic U (aU) phases (Klinkhammer and Palmer, 1991; Langmuir, 1978).

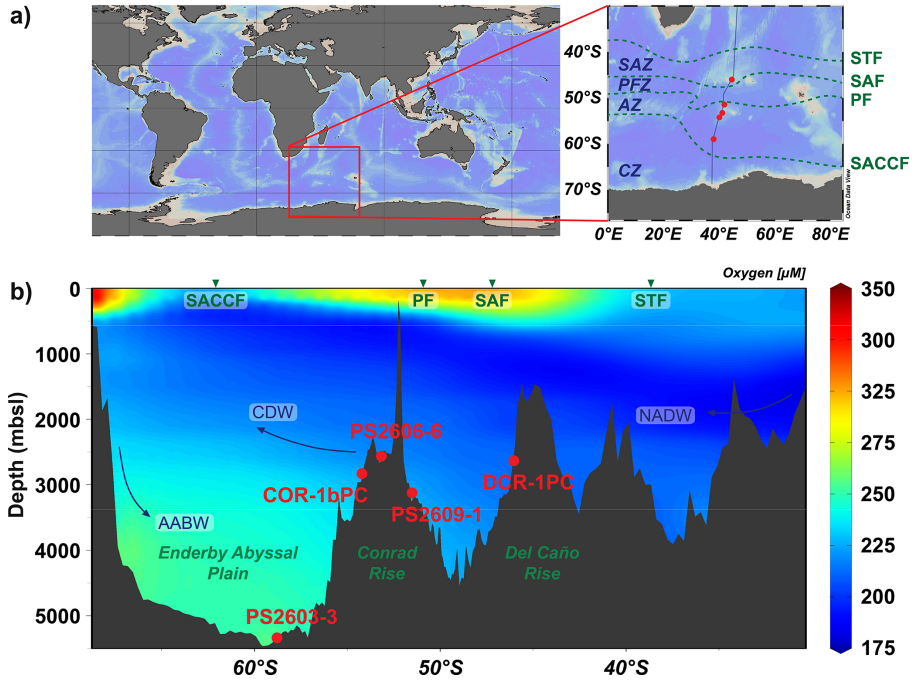

Figure 1. **(a)** Core locations in the SW Indian Ocean across the Southern Ocean frontal system. The fronts from north to south are the Subtropical Front (STF), Subantarctic Front (SAF), Polar Front (PF), and the Southern Antarctic Circumpolar Current Front (SACCF). The zones between them are defined as the Subantarctic Zone (SAZ), Polar Frontal Zone (PFZ), Antarctic Zone (AZ), and Continental Zone (CZ) (Orsi et al., 1995). **(b)** Cross section of core locations with modern oxygen concentrations (plotted with the ODV software, Schlitzer, 2018).

Table 1. Tie points of cores PS2609-1, PS2606-6, and PS2603-3. MagSus stands for magnetic susceptibility, $BSiO_2$ stands for biogenic silica, LR04 is the global benthic $\delta^{18}O$ LR04 stack (Lisiecki and Raymo, 2005), and EDC is Epica Dome C (Lambert et al., 2012).

Tie points PS2609-1

Depth (cm)	Age pointers (ka)	based on
0	0	
215	10	Ca peak
400	14	MagSus vs LR04; $BSiO_2$ vs LR04; Si/Ti vs LR04
785	28.68	Ti (XRF) vs EDC dust
808	29.88	Ti (XRF) vs EDC dust
1050	58.2	Ti (XRF) vs EDC dust
1145	71	MagSus vs LR04; Fe vs LR04
1157	72.25	Ti (XRF) vs EDC dust
1202	75.87	Ti (XRF) vs EDC dust
1293	83.6	Ti (XRF) vs EDC dust
1340	87	MagSus vs LR04; Fe vs LR04
1595	109	MagSus vs LR04; Fe vs LR04

Tie points PS2603-3

Depth (cm)	Age pointers (ka)	based on
0	0	
90	14	$BSiO_2$ vs LR04; rouxia lenenterae
405	109	$BSiO_2$ vs LR04; hemidiscus karstenii
545	130	$BSiO_2$ vs LR04
640	191	$BSiO_2$ vs LR04; rouxia constricta
690	243	$BSiO_2$ vs LR04
910	300	$BSiO_2$ vs LR04

Tie points PS2606-6

Depth (cm)	Age pointers (ka)	based on
0	0	
14	1.92	^{14}C - Xiao et al. (2016)
128	8.08	^{14}C - Xiao et al. (2016)
198	10.06	^{14}C - Xiao et al. (2016)
228	10.39	^{14}C - Xiao et al. (2016)
266	11.51	Ca/Ti (XRF) vs EDC dust
275	12.12	14C - Xiao et al. (2016)
328	12.79	Ca/Ti (XRF) vs EDC dust
357	14.52	^{14}C - Xiao et al. (2016)
380	15.07	Ca/Ti (XRF) vs EDC dust
427	19.68	^{14}C - Xiao et al. (2016)
478	20.56	Ti (XRF) vs EDC dust
559	24.67	Ti (XRF) vs EDC dust
591	26.20	Ti (XRF) vs EDC dust
639	29.20	Ti (XRF) vs EDC dust
719	44.39	Ti (XRF) vs EDC dust
725	45.44	Ti (XRF) vs EDC dust
786	55.27	Ti (XRF) vs EDC dust
844	67.90	MagSus vs LR04; Ti, Ca (XRF) vs EDC dust
889	71	MagSus vs LR04
905	73.30	Ca/Ti (XRF) vs EDC dust
936	75.87	Ti (XRF) vs EDC dust
968	78.93	Ca/Ti (XRF) vs EDC dust
1013	83.6	Ca/Ti (XRF) vs EDC dust
1036	87	MagSus vs LR04; Ti, Ca (XRF) vs EDC dust
1174	104.69	Ca/Ti (XRF) vs EDC dust
1210	109	MagSus vs LR04

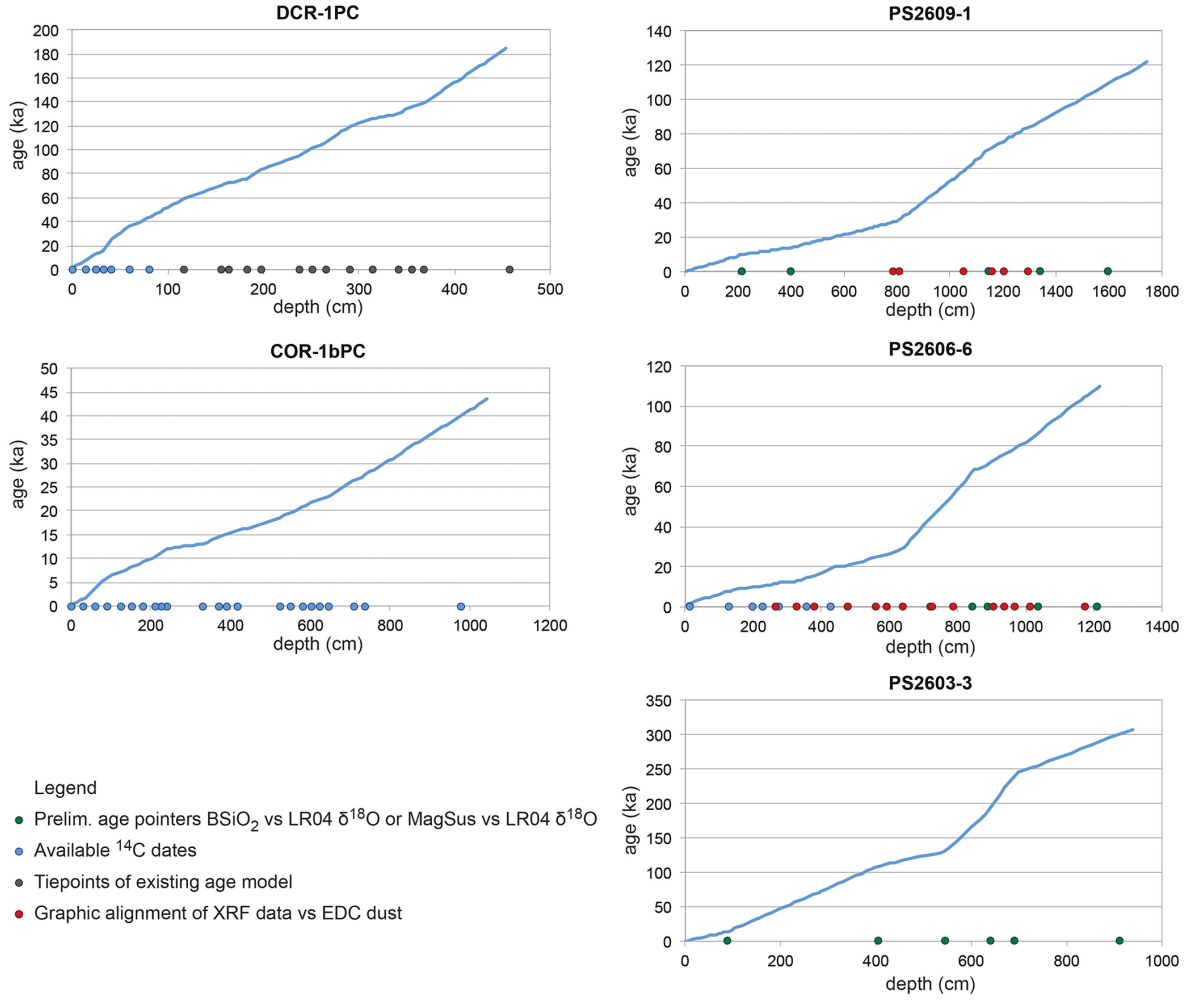

Figure 2. Age versus depth of each core.

The authigenic fraction of U can be determined by calculating the excess ^{238}U relative to detrital thorium (^{232}Th), which is done by assuming a constant, regionally informed detrital ^{238}U / ^{232}Th ratio. This ratio can vary locally, with lower values generally associated with crustal lithogenic sources. We considered a ratio of 0.5 for cores DCR-1PC, COR-1bPC, PS2909-1, and PS2909-6 (Francois et al., 2004; Henderson and Anderson, 2003). For PS2603-3, the core farthest to the south and potentially influenced by lithogenic material originating from the Antarctic continental crust, the minimum ^{238}U / ^{232}Th activity ratio observed is 0.27 ± 0.01. We therefore set the lithogenic end-member conservatively to 0.27.

$$\mathrm{aU} = A^{\mathrm{total}}_{\mathrm{U238}} - A^{\mathrm{total}}_{\mathrm{Th232}} \times \left(\frac{A_{\mathrm{U238}}}{A_{\mathrm{Th232}}}\right)^{\mathrm{det}} \quad (1)$$

The U and Th isotope compositions were quantified by isotope dilution following Anderson and Fleer (1982) and later modified by Choi et al. (2001), Pichat et al. (2004), and Lippold et al. (2009). Briefly, freeze-dried marine sediments (150–200 mg) were spiked (^{229}Th, ^{236}U) and completely digested in a pressure-assisted microwave ($T_{\mathrm{max}} = 180\,^{\circ}$C) using concentrated HNO_3, HCl, and HF. Both elements were separated and purified by anion exchange column chromatography using AG1-X8 resin. Measurements were conducted using a Thermo Fisher Scientific Neptune Plus multi-collector inductively coupled plasma mass spectrometer (MC-ICP-MS) at the University of Bern, and for the PS cores a single-collector ICP-MS (Thermo Fisher Scientific Element 2) at the Alfred Wegener Institute (AWI) in Bremerhaven was used. Internal standards were used in each batch to assess precision and reproducibility for the sample preparation process as well as for the measurements. Approximately half of the samples of cores PS2609-1, PS2606-6, and PS2603-3 had been prepared earlier following a similar procedure, albeit with slightly less sediment material (50 mg) and higher temperatures during digestion ($T_{\mathrm{max}} = 210\,^{\circ}$C). The chromatographic separation and subsequent purification of the U and Th fractions was performed using UTEVA resin (Eichrom). The isotope measurements were corrected with a

calibrated standard (UREM-11 Sarm 31) and yielded a relative standard deviation of less than 3.8 % and 3.5 % for ^{238}U and ^{234}U, respectively, and less than 5.7 % and 4.9 % for ^{230}Th and ^{232}Th, respectively. The measurement differences between the two mass spectrometers remain within these error ranges.

In marine sediments, manganese (Mn) precipitates under well-oxygenated conditions as oxyhydroxides (Mn(III) and (IV)) (Calvert and Pedersen, 1996). Manganese enrichments in sediments can be observed where the accumulation of organic matter is low and oxic conditions generally prevail (e.g., Calvert and Pedersen, 1993). Under more reducing conditions, the sedimentary distribution of Mn is controlled by the input of insoluble detrital fraction. Any Mn present in the sediment that is in excess relative to the concentration expected from the detrital fraction is assumed to have accumulated authigenically under oxic conditions. Here, we use the XRF core scanner peak intensity count ratios between Mn and Ti to constrain excess Mn, assuming a constant detrital ratio between both elements. Ti is assumed to be associated exclusively with lithogenic sources.

For Mn and Ti analyses in cores PS2609-1 and PS2606-6, the samples were fully digested, evaporated, and redissolved in 20 mL 1M HNO_3. An aliquot was then diluted 1 : 100, and rhodium was added as an internal standard. The Mn and Ti concentrations were measured on the single-collector ICP-MS (Thermo Fisher Scientific Element 2) at AWI in Bremerhaven. Reference material NIST 2702 was digested with each batch and measured with the samples. For cores COR-1bPC and DCR-1PC, the Mn and Ti measurements were acquired by XRF core logging with a Tatscan-F2 at the Kochi Core Center, Japan (Sakamoto et al., 2006).

2.4 Preserved opal export

The sedimentary biogenic opal fraction is predominantly composed of diatom frustules and minor amounts of radiolarians and sponge spicules. Diatoms dominate carbon export around and (mostly) south of the PF in the Southern Ocean (Cortese et al., 2004; Ragueneau et al., 2000). Sedimentary biogenic silica ($BSiO_2$), together with other proxies, has been widely used to reconstruct past changes in marine export production (e.g., Anderson et al., 2009; Bradtmiller et al., 2007; Chase et al., 2003). The accumulation of biogenic opal is influenced not only by opal production in the sunlit surface ocean but also by dissolution in the water column and at the seabed (Dezileau et al., 2003; Pondaven et al., 2000; Ragueneau et al., 2000). Empirical studies of modern opal export patterns suggest that the spatial distribution of opal burial predominantly reflects diatom productivity and opal export (e.g., Chase et al., 2003; Nelson et al., 2002; Pondaven et al., 2000; Sayles et al., 2001). However, the link between opal and carbon export is not straightforward, as other factors such as Fe availability can affect C and N uptake in diatoms relative to Si (Boutorh et al., 2016; Meyerink et al., 2017; Pichevin et al., 2014). A multi-proxy approach would provide a more unambiguous reconstruction of paleo-productivity in the region. However, based on the similar glacial–interglacial patterns of different paleo-productivity proxies in the region (Thöle et al., 2019), we assume that changes in biogenic opal fluxes provide a robust, first-order approximation of past changes in organic carbon delivery to the sediment.

Sedimentary biogenic opal concentrations were determined using Fourier transform infrared spectroscopy (FTIRS) at the University of Bern for cores DCR-1PC and COR-1bPC (Vogel et al., 2016). A laboratory-specific internal reference material was measured with each batch of samples to assess precision and reproducibility. For the PS cores, the sedimentary opal content was determined by alkaline extraction of silica according to Müller and Schneider (1993) at AWI, Bremerhaven. Both methods provide comparable results.

The ^{230}Th normalization approach was used to reconstruct vertical fluxes of $BSiO_2$. The method allows for accounting and correcting for potentially obfuscating effects, such as lateral sediment redistribution by bottom currents (Bourne et al., 2012; Costa et al., 2020; Francois et al., 2004; Henderson and Anderson, 2003). The flux of scavenged ^{230}Th (F^{230}Th) settling to the seafloor at a specific water depth z is assumed to be equal to its known production rate (β_{230}) from ^{234}U decay within the water column. The resultant inverse relationship between the scavenged ^{230}Th and the total vertical flux of particulate matter can be used to calculate preserved vertical fluxes ($^{\mathrm{pr}}F_{\mathrm{v}}$) from the activity of initial scavenged ^{230}Th in the sediment $\left(A^{\mathrm{scav}}_{\mathrm{Th230},(0)}\right)$.

$$^{\mathrm{pr}}F_{\mathrm{v}} = \frac{\beta_{230} \times z}{A^{\mathrm{scav}}_{\mathrm{Th230},(0)}} \tag{2}$$

The equation to derive the initial scavenged sedimentary ^{230}Th $\left(A^{\mathrm{scav}}_{\mathrm{Th230},(0)}\right)$ takes into account (i) ^{230}Th produced in situ from the decay of aU (^{238}U), (ii) ^{230}Th produced in situ from the decay of lithogenic U (^{238}U), and (iii) radiogenic decay of ^{230}Th after deposition. Normalizing the concentration of a specific sedimentary component (j) with the ^{230}Th approach provides a quantitative estimate of its preserved vertical flux $\left(^{\mathrm{pr}}F_j\right)$ through time:

$$^{\mathrm{pr}}F_j = {}^{\mathrm{pr}}F_{\mathrm{v}} \times f_j, \tag{3}$$

where f_j is the weight fraction of constituent j in the sediment.

3 Results

3.1 Subantarctic Zone of the SW Indian Ocean

3.1.1 Redox-sensitive metal records

The sedimentary aU concentrations in core DCR-1PC show the highest values of all cores (Fig. 3). The general pattern is consistent with a climate-related signal, with typically higher concentrations during cold periods and relatively low concentrations during warmer intervals. More specifically, the highest values occur during MIS 6 and MIS 3–MIS 2. During MIS 6 the values decrease gradually, show a peak around 130 ka, and then decrease steeply to levels well below 1 ppm at the start of MIS 5. The sedimentary aU concentrations are characterized by transient oscillations during MIS 5 (106–100, 88–85 ka), and concentrations then increase at the end of MIS 5 and stabilize during MIS 4. At the onset of MIS 3, aU levels increase steeply, with values remaining high throughout MIS 3, typically ranging between 5 and almost 8 ppm. Authigenic U concentrations start declining after 27 ka and reach the lowest levels of the entire glacial cycle at around 17.5 ka, remaining low throughout the Holocene. Mn is typically enriched during the two major warm climate intervals of MIS 5 and the Holocene, during which values are higher and show high-frequency variability, while Mn / Ti peak intensity count ratios hover around lower values during cold climate intervals, including a period between 115 and 100 ka.

3.1.2 Preserved opal export

Preserved biogenic opal fluxes vary between 0 and 0.7 g cm^{-2} kyr^{-1} (Fig. 3). Opal flux reconstructions show a pattern generally consistent with glacial–interglacial cyclicity, with typically higher opal fluxes during cold periods and lower fluxes during warmer climate intervals, consistent with paleoceanographic reconstructions from the region (Manoj and Thamban, 2015; Nair et al., 2019). Biogenic opal fluxes decrease about 5 ka before the onset of the glacial terminations during both MIS 6 and MIS 2.

There are distinct differences between the downcore aU and $BSiO_2$ flux records. During warm intervals and the transition into MIS 4, both aU and $BSiO_2$ flux records appear to be coupled, but at the start of MIS 3 both parameters start decoupling, suggesting a more nuanced relation between the two proxies.

3.2 Antarctic Zone of the SW Indian Ocean

3.2.1 Redox-sensitive metal records

In the following sections, the four cores retrieved from the Antarctic Zone of the Southern Ocean will be described from north to south wherever possible. The downcore sedimentary aU records vary similarly in all four cores (Fig. 4). Sedimentary aU concentrations vary between 0 and 3.5 ppm, with

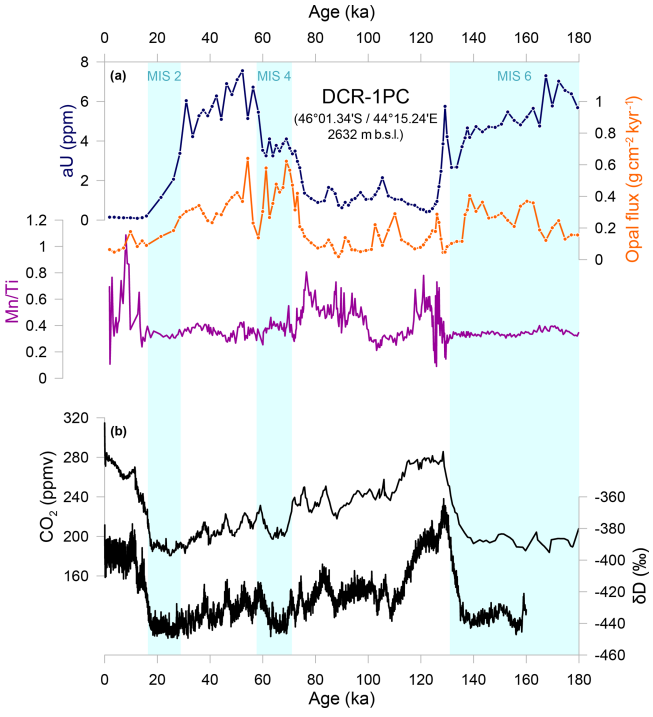

Figure 3. **(a)** Authigenic uranium concentrations (in blue), opal fluxes (in orange), and Mn / Ti ratios (in purple) from XRF scanning of sediment core DCR-1PC in the Subantarctic Zone. **(b)** Atmospheric CO_2 concentrations from EPICA Dome C ice core, the composite record (Bereiter et al., 2015, and references therein), and the δD record from EPICA Dome C ice core, reflecting Antarctic air temperatures (Jouzel et al., 2007). Light blue bars show cold periods MIS 2, 4, and 6 (Lisiecki and Raymo, 2005).

the southernmost core, PS2603-3, showing the lowest values and generally more subdued temporal variability. The lowest values in all cores are consistently found during MIS 5 and the Holocene. In both PS2609-1 and PS2606-6, sedimentary aU concentrations increase during MIS 4, a feature more salient in PS2609-1. Another increase mostly discernible in PS2609-1 is observed at the end of MIS 5 (85–80 ka). The low values during MIS 3 hover around 1 ppm in PS2609-1 and around 0.5 ppm in PS2606-6, respectively. In COR-1bPC, the core with the shortest sediment record, aU levels start increasing gently from the middle of MIS 3, before reaching highest values at the end of the last ice age just before the start of the deglacial transition.

The highest aU concentrations in cores PS2609-1, PS2606-6, and COR-1bPC occur during MIS 2 with a gradual increase from about 30 ka, peaking during the LGM. Thereafter, aU levels decline sharply to values well below 1 ppm at 2–4 ka, concomitant with the onset of the last glacial termination. After TERM I, a small increase around 11–8 ka is apparent. Throughout the Holocene, aU levels stay below 1 ppm. In PS2603-3 the highest values are also found within MIS 2, but the downcore variability is more muted. The de-

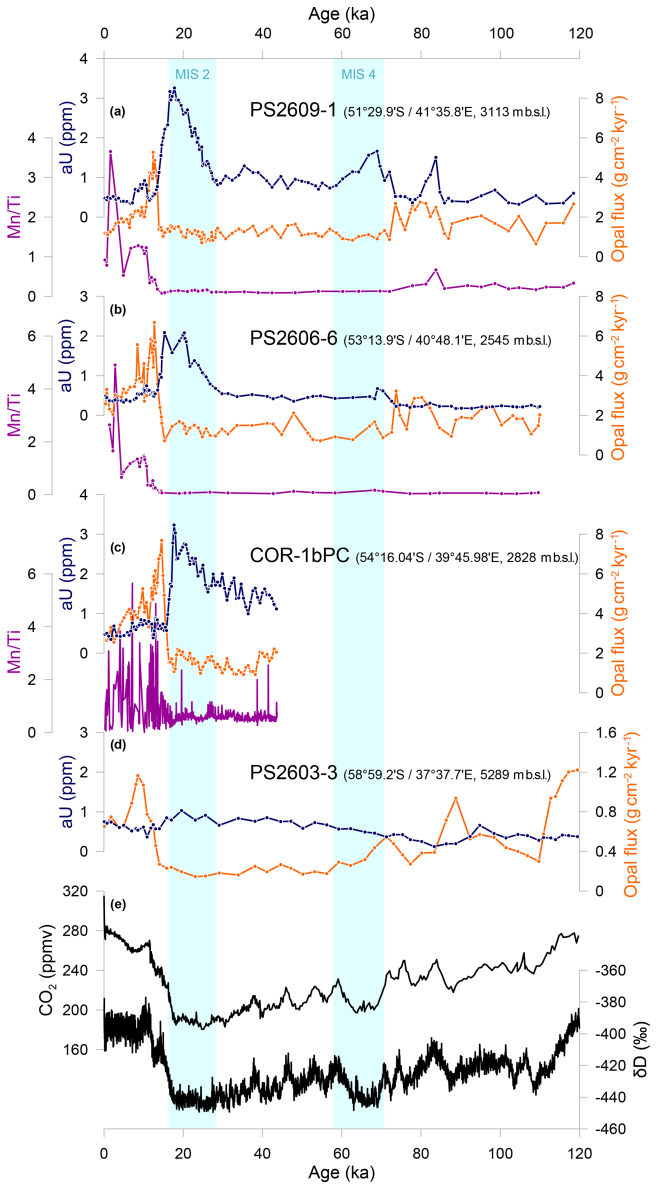

Figure 4. **(a–d)** Authigenic uranium concentrations (in blue), opal fluxes (in orange), and Mn / Ti ratios (in purple) in the Antarctic Zone south of the Polar Front. **(e)** Atmospheric CO_2 from the EPICA Dome C ice core, the composite record (Bereiter et al., 2015, and references therein), and the δD record from EPICA Dome C ice core, reflecting Antarctic air temperatures (Jouzel et al., 2007). Light blue bars show cold periods MIS 2 and 4 (Lisiecki and Raymo, 2005).

termination of sedimentary aU concentrations inherently assumes that the $^{238}U / ^{232}Th$ ratio of the lithogenic material supplied to the core site remained constant in space and time. Although the detrital $^{238}U / ^{232}Th$ ratio may have fluctuated in response to changing detrital sources (Manoj et al., 2012, 2013), the authigenic fraction typically amounts to $> 60\,\%$ of the total U. Such a decrease in the $^{238}U / ^{232}Th$ ratio during the last ice age would likely only marginally affect the absolute sedimentary aU concentrations and would not affect the first-order downcore patterns. Authigenic Mn levels remain low throughout the entire ice age and increase at the onset of the last glacial termination. The Mn / Ti records show similar trends, with low values during MIS 5 and MIS 4 and elevated or more variable values from about 15 ka.

3.2.2 Preserved opal export

The cores south of the PF show a consistent pattern, with relatively low preserved opal fluxes throughout most of MIS 2, 3, and 4; slight increases and higher variability during MIS 5; and a prominent peak after the LGM, all of which is consistent with available paleoceanographic records from the SW Indian Ocean (Manoj and Thamban, 2015; Nair et al., 2019). The values reached during this peak are much higher than in the SAZ, with values up to $4\,g\,cm^{-2}\,kyr^{-1}$. PS2603-3 shows the overall lowest values, reaching $1.2\,g\,cm^{-2}\,kyr^{-1}$ after both TERM I and II.

The downcore variations in $BSiO_2$ flux show a very different pattern than the aU records, especially during the LGM and TERM I. A rapid increase in $BSiO_2$ fluxes at the onset of the last deglaciation is observed at the same time as the aU decrease. After that point, $BSiO_2$ fluxes slowly decrease over the course of the Holocene. During MIS 5 there is a small increase in opal fluxes around 85–75 ka. The Mn / Ti values remain low in all cores and rise after the LGM in parallel with the $BSiO_2$ flux.

4 Interpretation and discussion

4.1 Dynamics of bottom water oxygenation in the SAZ

The downcore aU and Mn / Ti patterns are generally coherent (Fig. 3), and together the records provide a consistent picture reflecting past changes in bottom water oxygenation. Overall, the data indicate generally more reducing conditions during cold periods, whereas sediments were more oxidizing during warmer climate intervals, consistent with previous observations spanning the last deglacial transition in the region (Sruthi et al., 2012). The two redox-sensitive elements, however, are not perfectly anti-correlated, consistent with their inherent sensitivities to changing redox conditions (Tribovillard et al., 2006). When comparing both redox-sensitive metal records to opal fluxes, the proxies broadly allude to similar oxygenation conditions, in particular during glacial inception periods. However, towards peak glacial conditions the records show some degree of divergence.

The first drop in atmospheric pCO_2 at around 115 ka, marking the last glacial inception, coincides with a reduction in Mn / Ti values in core DCR-1PC, which could be attributed to a transition towards more reducing conditions (Fig. 3). At the transition from MIS 5 to MIS 4, both redox proxies show a clear shift towards more reducing conditions,

concomitant with a rise in biogenic opal export and coinciding with a substantial increase in dust and lithogenic and iron deposition rates recorded in Antarctic ice cores (e.g., Lambert et al., 2012) and subantarctic marine sediments (e.g., Anderson et al., 2014; Lamy et al., 2014; Manoj and Thamban, 2015; Martínez-García et al., 2014; Thöle et al., 2019). Kohfeld and Chase (2017) suggest a major change in ocean circulation, contemporaneous with this second drop in CO_2 centered at 72–65 ka. In particular, sedimentary neodymium (Nd) isotope records and ^{13}C data suggest a major reorganization of deep-ocean circulation at that time (e.g., Oliver et al., 2010; Wilson et al., 2015). Indeed, the shoaling of the Atlantic overturning cell may have left the abyssal ocean dominated by dense southern-sourced water (e.g., Lynch-Stieglitz et al., 2016; Matsumoto et al., 2002), which may have increased the vertical density gradient and contributed to isolate the deep ocean, making it more prone to sequester remineralized carbon (Hain et al., 2010; Skinner, 2009; Yu et al., 2016). We therefore suggest that both increased export production and by inference organic matter respiration, as well as a decrease in deep-ocean ventilation, preconditioned the sediments, maintaining sufficiently reducing conditions to allow for recording the more subtle ventilation changes of the last ice age (Gottschalk et al., 2020a).

The decrease in sedimentary aU concentrations and associated reoxygenation of bottom waters started within MIS 2 and not, as expected, towards the end of the last ice age, when ocean circulation and upwelling began to intensify as the Southern Hemisphere warmed (Basak et al., 2018; Gottschalk et al., 2016, 2020b; Jaccard et al., 2016; Rae et al., 2018; Ronge et al., 2020; Skinner et al., 2010). Rather than a regionally disparate initiation of upwelling, the decrease in aU accumulation in core DCR-1PC may be related to diagenetic "burn-down". Diagenetic redeposition of sedimentary aU is indeed observed when oxygenated conditions in the uppermost layers of the sediment recur (e.g., Thomson et al., 1990), for example as a result of reinvigorating deep-water ventilation. As oxygen diffuses into pore waters, previously precipitated U will dissolve and will be either lost to the overlying water or diffuse deeper into the sediment, where conditions are still reducing and where it will be reprecipitated (Colley et al., 1989; Jacobel et al., 2017; Mangini et al., 2001). A high sediment accumulation rate would limit the depth interval over which burn-down would affect the downcore aU record. Core DCR-1PC has the lowest sedimentation rates of the five cores investigated and thus is potentially more prone to be affected by oxidative burn-down (Korff et al., 2016). With the lowest sedimentation rate within the core being reported between 17 and 25 ka (< 1 cm kyr^{-1}, Fig. 5), re-dissolution provides a plausible explanation accounting for the early aU decrease. Alternatively, the observed decrease in aU concentrations during the LGM may reveal a transient sedimentary hiatus, which may have affected the sedimentary record in this core. During the penultimate glacial termination (TERM II), aU appears to have

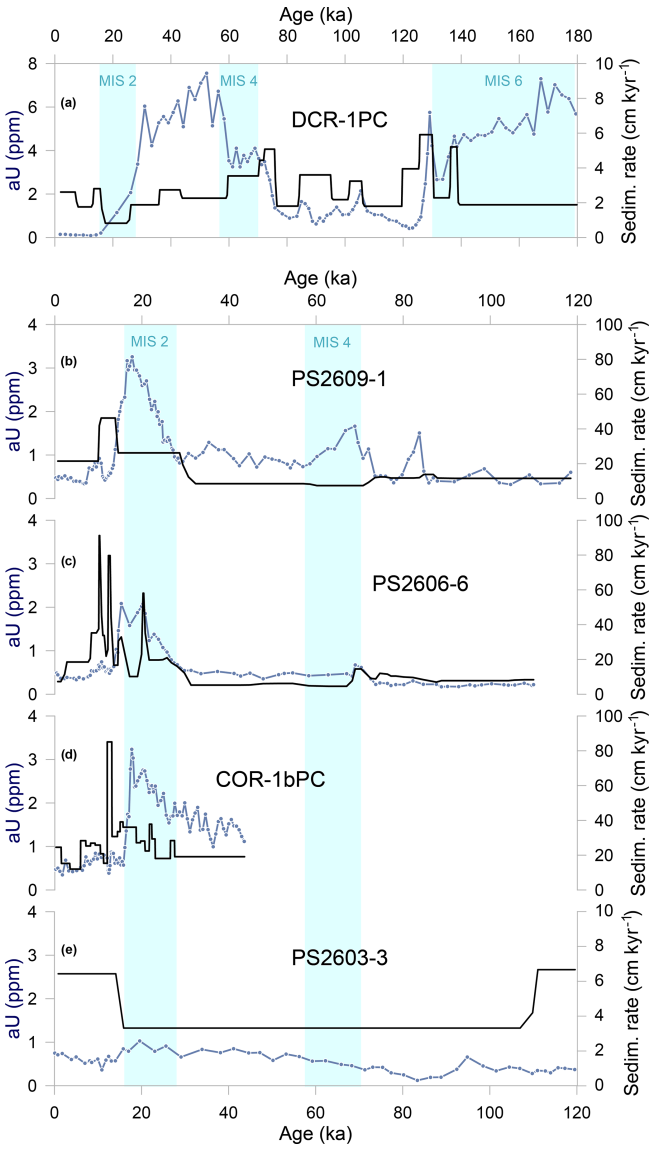

Figure 5. (a–e) Sedimentation rates (in black) and authigenic uranium concentrations (in light blue) in all cores from north to south. Light blue bars show cold periods MIS 2, 4, and 6 (Lisiecki and Raymo, 2005).

only been marginally affected by remobilization processes. The sedimentation rates during this interval are indeed higher than at the end of the last ice age (Fig. 5).

The early decrease in $bSiO_2$ export towards the end of both glacial periods could be related to increasingly complete $Si(OH)_4$ consumption south of the Polar Front (Dumont et al., 2020). Upwelling and thus nutrient supply to the surface water south of the PF were substantially reduced during glacial times (Anderson et al., 2009; Francois et al., 1997). Biological productivity was reduced, but at the same time nitrate consumption was more complete (Ai et al., 2020; Studer et al., 2015), stemming CO_2 outgassing from

the ocean interior. Part of these surface waters are transported towards the north, and when they reach the location of DCR-1PC they are largely depleted of $Si(OH)_4$. Transitioning towards peak glacial conditions, there would have been gradually less $Si(OH)_4$ available for opal production in the SAZ, as reflected by the downcore opal flux records. Relaxed Fe limitation as a result of enhanced bioavailable Fe input with dust would have lowered the Si / N uptake ratio in diatoms (Brzezinski et al., 2002). Nitrogen isotope studies show that nitrate utilization was more complete in glacial periods when compared to interglacials (Ai et al., 2020; Horn et al., 2011; Martínez-García et al., 2014; Studer et al., 2015), whereas silicon isotopes show an opposite pattern (Brzezinski et al., 2002; Dumont et al., 2020). Despite preferred nitrate uptake and therefore potentially more silicate leakage towards the north, the overall amount of $Si(OH)_4$ upwelled from depth might have been declining, thus limiting diatom growth (Brzezinski et al., 2002; Dumont et al., 2020). Moreover, as the age model and the low sedimentation rate may indicate, a possible hiatus during this critical interval may provide a complementary explanation to account for the early decrease in opal fluxes.

4.2 Dynamics of bottom water oxygenation in the AZ

South of the PF, all cores, with the exception of the slowly accumulating core retrieved from Enderby Basin, record similar (paleo)oceanographic evolutions. The sedimentary aU and Mn / Ti levels show a consistent downcore pattern with generally more reducing conditions during peak glacial times and rapid (re)oxygenation during glacial terminations. These observations are consistent with recent radiocarbon-based evidence suggesting that the deep Indian Ocean was generally more poorly ventilated during the last ice age (Bharti et al., 2022; Gottschalk et al., 2020b; Ronge et al., 2020). Preserved opal fluxes are persistently low during cold periods, while aU and Mn / Ti values are consistent with increasingly reducing conditions. The rapid increase in preserved opal fluxes coinciding with more oxygenated conditions during TERM I imply that export production and thus the respiratory demand for organic matter remineralization only played a secondary role, whereas ventilation imposed a primary control on sedimentary oxygenation levels. The rapid increase in biogenic opal fluxes at the onset of both glacial terminations is likely a result of enhanced upwelling of subsurface waters, rich in both (micro)nutrients and CO_2 (Anderson et al., 2009; Gottschalk et al., 2020b; Jaccard et al., 2016; Skinner et al., 2010).

With the available data of redox-sensitive elements U and Mn and the preserved opal fluxes in these cores, an alternative interpretation needs to be considered. As Fe scarcity reduces the C and N uptake ratio relative to Si (Boutorh et al., 2016; Meyerink et al., 2017; Pichevin et al., 2014), the opal peak during the deglaciation can at least partly be attributed to Fe limitation, which is possibly induced by a reduction of Fe-bearing dust input. To further explore this alternative possibility, downcore changes in Si / Fe ratios in diatom shells could be analyzed. However, considering multi-proxy studies of export production in the AZ (e.g., Chase et al., 2003; Thöle et al., 2019) and enhanced upwelling intensities during the deglacial (e.g., Basak et al., 2018; Gottschalk et al., 2020b; Ronge et al., 2020; Skinner et al., 2010), we suggest the observed opal peak to be the result of increased production due to enhanced nutrient availability from upwelled deep waters, in line with a meridional shift of the Southern Ocean frontal system.

Reinvigorating ventilation in the Southern Ocean associated with the glacial termination would leave a spatially coherent oxygenation pattern in all cores, as it was related to an overall reorganization in ocean circulation. The associated opal signal might slightly differ in time given that the upwelling region shifts along with the frontal system (Anderson et al., 2009). However, as the timing of aU peak emplacement cannot robustly be defined and the sampling resolution may be insufficient, the potential time lag between the onset of the aU decrease and the sharp rise in opal production and deposition cannot reliably be assessed.

In the southernmost core PS2603-3, aU and preserved opal fluxes suggest similar oceanographic dynamics in the Enderby Abyssal Plain. The opal peak that is concomitant with the onset of TERM I suggests that the core is similarly recording enhanced upwelling, but the maximum values of $1.2\,g\,cm^{-2}\,kyr^{-1}$ are consistent with the core being located further away from the most vigorous upwelling region. The slight increase in the aU record during the glacial maxima suggests that bottom water oxygenation was generally reduced during ice ages.

4.3 Ventilation and circulation changes on glacial–interglacial timescales and their impact on atmospheric pCO_2

Across the transect, the core site locations are bathed by different water masses (Fig. 1). With the exception of the southernmost core, which is bathed by Antarctic Bottom Water (AABW), the other four sediment cores are located in Circumpolar Deep Water (CDW), which is formed partly from North Atlantic Deep Water (NADW) and mixed with AABW and other deep waters that originate from the Indian and Pacific oceans (Talley, 2013). CDW is upwelled in the Southern Ocean along tilted isopycnals. The lower CDW, which stems mainly from dense, high-salinity NADW, then moves towards the south as a precursor for AABW. The less dense upper CDW, which has a more oxygen-depleted signature from older Indian and Pacific deep waters, is transported to the north by Ekman flow (Talley, 2013). The lower and upper CDW thus have distinct oxygen concentrations, but the range in dissolved oxygen concentration changes is smaller than the ranges reported for the last glacial cycle due to increased carbon sequestration (Anderson et al., 2019; Galbraith and

Skinner, 2020). Therefore, any variations in aU and Mn / Ti values are unlikely to be primarily driven by local variations in oxygenation, but rather record a coherent regional picture. The main factor controlling changes in oxygenation at the sediment–water interface and in pore waters is thus more likely related to bottom water ventilation changes. This can be argued for by the decoupling of aU and opal fluxes in DCR-1PC (Fig. 3) during the later phase of the glacial periods and by the more pronounced anti-phasing in the records south of the PF. This anti-phasing at TERM I with invigorated circulation and thus rejuvenation of the deep ocean is linked to enhanced supply of nutrient-rich waters to the surface, which in turn fueled biological production. However, this nutrient-fueled phytoplankton growth was not efficient to quantitatively fix dissolved carbon, thus allowing CO_2 to escape to the atmosphere (Ai et al., 2020; Sigman et al., 2010; Studer et al., 2015). The increase in opal fluxes in connection with more ventilated bottom waters at the end of the glacial periods fits well with higher atmospheric CO_2 inventories associated with the release of previously sequestered carbon from subsurface waters (Burke and Robinson, 2012; Jaccard et al., 2016; Ronge et al., 2020; Skinner et al., 2010).

The major slowdown in deep-ocean circulation occurred mostly after the MIS 5–MIS 4 transition. Before this point, at the onset of the glacial period, other factors may have contributed to the drawdown of atmospheric carbon. During the first CO_2 drop within MIS 5, cooling sea surface temperatures at high latitudes in both hemispheres led to CO_2 reduction through barrier mechanisms. Sea ice formation and seasonally induced meltwater would lead to stronger surface water stratification and affect air–sea gas exchange and impede the ability of lower waters to rise to the productive surface (Watson and Naveira Garabato, 2006; Wolff et al., 2010). This barrier mechanism is consistent with the observed first increase in nitrate consumption associated with enhanced stratification of the surface ocean (Ai et al., 2020; Studer et al., 2015). Only at the second CO_2 drop at the MIS 5–MIS 4 transition does deep-ocean circulation slow down, as indicated by increased aU and decreased Mn / Ti, in good agreement with other proxy data (Jimenez-Espejo et al., 2020; Kohfeld and Chase, 2017; Oliver et al., 2010; Wilson et al., 2015). This second drop was accompanied by enhanced biological export production north of the PF fueled by enhanced dust input (Lambert et al., 2012). Our results show a regionally coherent increase in sedimentary aU concentrations, especially after the MIS 5–MIS 4 transition, and indicate the gradually more sluggish overturning circulation that contributed to partitioning carbon into the ocean interior (Gottschalk et al., 2020a; Jaccard et al., 2016, 2013; Kohfeld and Chase, 2017).

South of the PF (in core PS2609-1), the aU record indicates reoxygenation during MIS 3, while in the SAZ reducing conditions intensify. This contrasting behavior could be explained by a reorganization of deep-water masses. NADW that forms CDW in which our cores are located could have retracted northwards during MIS 3, while AAWB, which is generally more oxygenated than NADW, bathed the cores south of the PF (Sigman et al., 2010). Progressing towards the glacial maximum, the upwelled water masses would successively be more isolated from atmospheric forcing by extended sea ice, leading to more oxygen-depleted and carbon-rich AABW (Ferrari et al., 2014), and thus resulting in the increased aU levels in the southern cores during MIS 2.

5 Conclusions

Five marine sediment cores from the Indian sector of the Southern Ocean were considered in this study. They were retrieved across a transect spanning a latitudinal band of about 15° from Del Caño Rise (north of the SAF), Conrad Rise, and as far south as the Enderby Abyssal Plain, which is close to the Southern ACC Front (SACCF). Redox-sensitive aU and Mn / Ti ratios were studied in detail and compared to ^{230}Th-normalized preserved opal export fluxes to better constrain bottom water oxygenation in the context of carbon sequestration since the last glacial inception. Our results suggest that more sluggish circulation dynamics and thus ventilation changes are the major contributor accounting for enhanced carbon sequestration in deep-water masses during glacial periods. Our paleoceanographic records covering a meridional transect increase the spatial resolution of deep-water oxygenation records in the Southern Ocean and are overall in agreement with previous reconstructions from other deep-water sites (Chase et al., 2001; Dezileau et al., 2002; Francois et al., 1997; Frank et al., 2000; Gottschalk et al., 2020b; Jaccard et al., 2016; Thöle et al., 2019).

The influence of locally enhanced biological export production on oxygenation states due to increased Fe fertilization by dust input cannot be ruled out completely, especially in the SAZ and at the transition from MIS 5 to 4 (Jaccard et al., 2016, 2013; Martínez-García et al., 2014). In the AZ, however, export production likely played a minor role in partitioning carbon from the atmosphere. More importantly, decreased ventilation and the associated slowdown of overall ocean circulation during cold periods (Wu et al., 2021) led to more carbon being sequestered in the ocean interior. Our results indicate a major drawdown of atmospheric CO_2 by a more sluggish overturning circulation. The most substantial circulation changes are suggested to have occurred at the transition of MIS 5–MIS 4, as has been proposed by Kohfeld and Chase (2017). South of the PF, reducing conditions recede during MIS 3, most likely due to a reorganization of deep-water circulation with larger expansion of AABW, reaching the southern core locations (Ferrari et al., 2014). Later during MIS 2, these deep waters that upwell to newly form AABW were also increasingly isolated from atmospheric forcing due to expanded sea ice cover. Generally, our reconstructions support the hypothesis that ventilation dynamics are the main driver of oxygenation changes

in the Southern Ocean and thus exert a major control on the air–sea partitioning of CO_2 over the last glacial cycle.

Data availability. The data set of this study is accessible on BORIS portal: https://doi.org/10.48620/69 (Amsler, 2022).

Author contributions. HEA and SLJ devised the study. HEA, LMT, IS, and WG carried out U / Th measurements. HEA and GK carried out biogenic opal measurements. IS and WG conducted the absolute Mn and Ti measurements. OE contributed largely to the age models for the PS cores. MI and GK planned the cruises and provided access to the core material and XRF measurements. HEA wrote the initial version of the manuscript, and all co-authors contributed to the manuscript.

Competing interests. The contact author has declared that none of the authors has any competing interests.

Disclaimer. Publisher's note: Copernicus Publications remains neutral with regard to jurisdictional claims in published maps and institutional affiliations.

Acknowledgements. We thank the captain, crew members, and scientists of the R/V *Hakuho-maru* and R/V *Polarstern* for the recovery of the sediment cores during the KH-10-7 (lead scientist: Minoru Ikehara) and ANT-XI/4 cruises (lead scientist: Gerhard Kuhn) in the Southern Ocean. We thank Martin Wille, Igor Villa, Jörg Rickli, David Janssen, Edel O'Sullivan, Alessandro Maltese, and Jörg Lippold for their help with the MC-ICP-MS measurements; Julijana Krbanjevic and Hendrik Vogel for helping with the opal measurements; and Takuya Matsuzaki for the Tatscan measurements. Funding for this study was provided by the Swiss National Science Foundation (grant nos. PP00P2_144811 and 200021_163003). Oliver Esper, Walter Geibert, Gerhard Kuhn, and Ingrid Stimac were funded by the Alfred-Wegener-Institut Helmholtz-Zentrum für Polar- und Meeresforschung PACES II research program. Minoru Ikehara was funded by the Japan Society for the Promotion of Science KAKENHI (Grants-in-Aid for Scientific Research P23244102 and JP17H06318). The isotope data were obtained on a Neptune MC-ICP-MS acquired with funds from NCCR PlanetS, supported by the Swiss National Science Foundation (grant no. 51NF40-141881).

Financial support. This research has been supported by the Swiss National Science Foundation (grant nos. PP00P2_144811 and 200021_163003).

Review statement. This paper was edited by Luc Beaufort and reviewed by two anonymous referees.

References

Adkins, J. F.: The role of deep ocean circulation in setting glacial climates, Paleoceanography, 28, 539–561, https://doi.org/10.1002/palo.20046, 2013.

Adkins, J. F., McIntyre, K., and Schrag, D. P.: The salinity, temperature, and δ18O of the glacial deep ocean, Science, 298, 69–73, https://doi.org/10.1126/science.1076252, 2002.

Ai, X. E., Studer, A. S., Sigman, D. M., Martínez-García, A., Fripiat, F., Thöle, L. M., Michel, E., Gottschalk, J., Arnold, L., Moretti, S., Schmitt, M., Oleynik, S., Jaccard, S. L., and Haug, G. H.: Southern Ocean upwelling, Earth's obliquity, and glacial-interglacial atmospheric CO_2 change, Science, 370, 1348–1352, https://doi.org/10.1126/science.abd2115, 2020.

Amsler, H. E.: Paleoceanographic dynamics of the Southern Indian Ocean reconstructed from geochemical and sedimentological proxies across the last glacial cycle, BORIS [data set], https://doi.org/10.48620/69, 2022.

Anderson, R. F. and Fleer, A. P.: Determination of Natural Actinides and Plutonium in Marine Particulate Material, Anal. Chem. 54, 1142–1147, https://doi.org/10.1021/ac00244a030, 1982.

Anderson, R. F., Ali, S., Bradtmiller, L. I., Nielsen, S. H. H., Fleisher, M. Q., Anderson, B. E., and Burckle, L. H.: Wind-driven Upwelling in the Southern Ocean and the Deglacial Rise in Atmospheric CO_2, Science, 323, 1443–1448, https://doi.org/10.1126/science.1167441, 2009.

Anderson, R. F., Barker, S., Fleisher, M., Gersonde, R., Goldstein, S. L., Kuhn, G., Mortyn, P. G., Pahnke, K., and Sachs, J. P.: Biological response to millennial variability of dust and nutrient supply in the Subantarctic South Atlantic Ocean, Philos. Trans. Roy. Soc. A, 372, 20130054, https://doi.org/10.1098/rsta.2013.0054, 2014.

Anderson, R. F., Sachs, J. P., Fleisher, M. Q., Allen, K. A., Yu, J., Koutavas, A., and Jaccard, S. L.: Deep-sea oxygen depletion and ocean carbon sequestration during the last ice age, Global Biogeochem. Cy., 33, 301–317, https://doi.org/10.1029/2018GB006049, 2019.

Bard, E.: Correction of accelerator mass spectrometry ^{14}C ages measured in planktic foraminifera: paleoceanographic implications, Paleoceanography, 3, 635–645, https://doi.org/10.1029/PA003i006p00635, 1988.

Basak, C., Fröllje, H., Lamy, F., Gersonde, R., Benz, V., Anderson, R. F., Molina-Kescher, M., and Pahnke, K.: Breakup of last glacial deep stratification in the South Pacific, Science, 359, 900–904, https://doi.org/10.1126/science.aao2473, 2018.

Bauska, T. K., Baggenstos, D., Brook, E. J., Mix, A. C., Marcott, S. E., Petrenko, V. V., Schaefer, H., Severinghaus, J. P., and Lee, J. E.: Carbon isotopes characterize rapid changes in atmospheric carbon dioxide during the last deglaciation, P. Natl. Acad. Sci. USA, 113, 13, https://doi.org/10.1073/pnas.1513868113, 2016.

Bereiter, B., Eggleston, S., Schmitt, J., Nehrbass-Ahles, C., Stocker, T. F., Fischer, H., Kipfstuhl, S., and Chappellaz, J.: Revision of the EPICA Dome C CO_2 record from 800 to 600 kyr before present, Geophys. Res. Lett., 42, 542–549, https://doi.org/10.1002/2014GL061957, 2015.

Bharti, N., Bhushan, R., Skinner, L. C., Muruganantham, M., Jena, P. S., Dabhi, A., and Shivama, A.: Evidence of poorly ventilated deep Central Indian Ocean during

the last glaciation, Earth Planet. Sci. Lett., 582, 117438, https://doi.org/10.1016/j.epsl.2022.117438, 2022.

Bourne, M. D., Thomas, A. L., Mac Niocaill, C., and Henderson, G. M.: Improved determination of marine sedimentation rates using $^{230}Th_{xs}$, Geochem. Geophy. Geosy., 13, 1, https://doi.org/10.1029/2012GC004295, 2012.

Boutorh, J., Moriceau, B., Gallinari, M., Ragueneau, O., and Bucciarelli, E.: Effect of trace metal-limited growth on the postmortem dissolution of the marine diatom Pseudonitzschia delicatissima, Global Biogeochem. Cy., 30, 57–69, https://doi.org/10.1002/2015GB005088, 2016.

Bouttes, N., Paillard, D., and Roche, D. M.: Impact of brine-induced stratification on the glacial carbon cycle, Clim. Past, 6, 575–589, https://doi.org/10.5194/cp-6-575-2010, 2010.

Bradtmiller, L. I., Anderson, R. F., Fleisher, M. Q., and Burckle, L. H.: Opal burial in the equatorial Atlantic Ocean over the last 30 ka: Implications for glacial-interglacial changes in the ocean silicon cycle, Paleoceanography, 22, PA4216, https://doi.org/10.1029/2007PA001443, 2007.

Brzezinski, M. A., Pride, C. J., Franck, V. M., Sigman, D. M., Matsumoto, K., Gruber, N., Rau, G. H., and Coale, K. H.: A switch from $Si(OH)_4$ to NO_3^- depletion in the glacial Southern Ocean, Geophys. Res. Lett., 29, 1564, https://doi.org/10.1029/2001GL014349, 2002.

Burke, A. and Robinson, L. F.: The Southern Ocean's Role in Carbon Exchange During the Last Deglaciation, Science, 335, 557–561, https://doi.org/10.1126/science.1208163, 2012.

Butzin, M., Prange, M., and Lohmann, G.: Radiocarbon simulations for the glacial ocean: The effects of wind stress, Southern Ocean sea ice and Heinrich events, Earth Planet. Sci. Lett., 235, 45–61, https://doi.org/10.1016/j.epsl.2005.03.003, 2005.

Calvert, S. E. and Pedersen, T. F.: Geochemistry of Recent oxic and anoxic marine sediments: Implications for the geological record, Mar. Geol., 113, 67–88, https://doi.org/10.1016/0025-3227(93)90150-T, 1993.

Calvert, S. E. and Pedersen, T. F.: Sedimentary geochemistry of manganese: Implications for the environment of formation of manganiferous black shales, Econ. Geol., 91, 36–47, https://doi.org/10.2113/gsecongeo.91.1.36, 1996.

Chase, Z., Anderson, R. F., and Fleisher, M. Q.: Evidence from authigenic uranium for increased productivity of the glacial Subantarctic Ocean, Paleoceanography, 16, 5, 468–478, https://doi.org/10.1029/2000PA000542, 2001.

Chase, Z., Anderson, R. F., Fleisher, M. Q., and Kubik, P. W.: Accumulation of biogenic and lithogenic material in the Pacific sector of the Southern Ocean during the past 40,000 years, Deep. Res. Part II Top. Stud. Oceanogr, 50, 799–832, https://doi.org/10.1016/S0967-0645(02)00595-7, 2003.

Choi, M. S., Francois, R., Sims, K., Bacon, M. P., Brown-Leger, S., Fleer, A. P., Ball, L., Schneider, D., and Pichat, S.: Rapid determination of ^{230}Th and ^{231}Pa in seawater by desolvated micro-nebulization Inductively Coupled Plasma magnetic sector mass spectrometry, Mar. Chem., 76, 99–112, https://doi.org/10.1016/S0304-4203(01)00050-0, 2001.

Colley, S., Thomson, J., and Toole, J.: Uranium relocations and derivation of quasi-isochrons for a turbidite/pelagic sequence in the Northeast Atlantic, Geochim. Cosmochim. Acta, 53, 1223–1234, https://doi.org/10.1016/0016-7037(89)90058-6, 1989.

Cortese, G., Gersonde, R., Hillenbrand, C. D., and Kuhn, G.: Opal sedimentation shifts in the World Ocean over the last 15 Myr, Earth Planet. Sci. Lett., 224, 509–527, https://doi.org/10.1016/j.epsl.2004.05.035, 2004.

Costa, K. M., Hayes, C. T., Anderson, R. F., Pavia, F. J., Bausch, A., Deng, F., Dutay, J. C., Geibert, W., Heinze, C., Henderson, G., Hillaire-Marcel, C., Hoffmann, S., Jaccard, S. L., Jacobel, A. W., Kienast, S. S., Kipp, L., Lerner, P., Lippold, J., Lund, D., Marcantonio, F., McGee, D., McManus, J. F., Mekik, F., Middleton, J. L., Missiaen, L., Not, C., Pichat, S., Robinson, L. F., Rowland, G. H., Roy-Barman, M., Tagliabue, A., Torfstein, A., Winckler, G., and Zhou, Y.: ^{230}Th normalization: New insights on an essential tool for quantifying sedimentary fluxes in the modern and Quaternary ocean, Paleoceanogr. Paleoclimatol., 35, e2019PA003820, https://doi.org/10.1029/2019PA003820, 2020.

Crosta, X., Shukla, S. K., Ther, O., Ikehara, M., Yamane, M., and Yokoyama, Y.: Last Abundant Appearance Datum of Hemidiscus karstenii driven by climate change, Mar. Micropaleontol., 157, 101861, https://doi.org/10.1016/j.marmicro.2020.101861, 2020.

Dezileau, L., Bareille, G., and Reyss, J.-L.: Enrichissement en uranium authigène dans les sédiments glaciaires de l'océan Austral, C. R. Geoscience, 334, 1039–1046, https://doi.org/10.1016/S1631-0713(02)01826-6, 2002.

Dezileau, L., Reyss, J.-L., and Lemoine, F.: Late Quaternary changes in biogenic opal fluxes in the Southern Indian Ocean, Mar. Geol., 202, 143–158, https://doi.org/10.1016/S0025-3227(03)00283-4, 2003.

Dumont, M., Pichevin, L., Geibert, W., Crosta, X., Michel, E., Moreton, S., Dobby, K., and Ganeshram, R.: The nature of deep overturning and reconfigurations of the silicon cycle across the last deglaciation, Nat. Commun., 11, 1534, https://doi.org/10.1038/s41467-020-15101-6, 2020.

Durgadoo, J. V., Lutjeharms, J. R. E., Biastoch, A., and Ansorge, I. J.: The Conrad Rise as an obstruction to the Antarctic Circumpolar Current, Geophys. Res. Lett., 35, L20606, https://doi.org/10.1029/2008GL035382, 2008.

Ferrari, R., Jansen, M. F., Adkins, J. F., Burke, A., Stewart, A. L., and Thompson, A. F.: Antarctic sea ice control on ocean circulation in present and glacial climates, P. Natl. Acad. Sci. USA, 111, 24, 8753–8758, https://doi.org/10.1073/pnas.1323922111, 2014.

Francois, R., Altabet, M. A., Yu, E.-F., Sigman, D. M., Bacon, M. P., Frank, M., Bohrmann, G., Bareille, G., and Labeyrie, L. D.: Contribution of Southern Ocean surface-water stratification to low atmospheric CO_2 concentrations during the last glacial period, Nature, 389, 929–935, https://doi.org/10.1038/40073, 1997.

Francois, R., Frank, M., Rutgers van der Loeff, M. M., and Bacon, M. P.: ^{230}Th normalization: An essential tool for interpreting sedimentary fluxes during the late Quaternary, Paleoceanography, 19, PA1018, https://doi.org/10.1029/2003pa000939, 2004.

Frank, M., Gersonde, R., Rutgers van der Loeff, M. M., Bohrmann, G., Nürnberg, C. C., Kubik, P. W., Suter, M., and Mangini, A.: Similar glacial and interglacial export bioproductivity in the Atlantic sector of the Southern Ocean: Multiproxy evidence and implications for glacial atmospheric CO_2, Paleoceanography, 15, 642–658, https://doi.org/10.1029/2000PA000497, 2000.

Galbraith, E. D. and Jaccard, S. L.: Deglacial weakening of the oceanic soft tissue pump: Global constraints from sedimentary nitrogen isotopes and oxygenation proxies, Quaternary Sci. Rev.,

109, 38–48, https://doi.org/10.1016/j.quascirev.2014.11.012, 2015.

Galbraith, E. D. and Skinner, L. C.: The Biological Pump During the Last Glacial Maximum, Annu. Rev. Mar. Sci., 12, 559–586, https://doi.org/10.1146/annurev-marine-010419-010906, 2020.

Galbraith, E. D., Young Kwon, E., Bianchi, D., Hain, M. P., and Sarmiento, J. L.: The impact of atmospheric pCO_2 on carbon isotope ratios of the atmosphere and ocean, Global Biogeochem. Cy., 29, 307–324, https://doi.org/10.1002/2014GB004929, 2015.

Geibert, W., Stimac, I., Rutgers van der Loeff, M. M., and Kuhn, G.: Dating Deep-Sea Sediments With ^{230}Th Excess Using a Constant Rate of Supply Model, Paleoceanogr. Paleoclimatology, 34, 1895–1912, https://doi.org/10.1029/2019PA003663, 2019.

Gottschalk, J., Skinner, L. C., Lippold, J., Vogel, H., Frank, N., Jaccard, S. L., and Waelbroeck, C.: Biological and physical controls in the Southern Ocean on past millennial-scale atmospheric CO_2 changes, Nat. Commun., 7, 11539, https://doi.org/10.1038/ncomms11539, 2016.

Gottschalk, J., Skinner, L. C., Jaccard, S. L., Menviel, L., Nehrbass-Ahles, C., and Waelbroeck, C.: Southern Ocean link between changes in atmospheric CO_2 levels and northern-hemisphere climate anomalies during the last two glacial periods, Quaternary Sci. Rev., 230, 106067, https://doi.org/10.1016/j.quascirev.2019.106067, 2020a.

Gottschalk, J., Michel, E., Thöle, L. M., Anja S. Studer, A. S., Hasenfratz, A. P., Schmid, N., Butzin, M., Mazaud, A., Martínez-García, A., Szidat, S., and Jaccard, S. L.: Glacial heterogeneity in Southern Ocean carbon storage abated by fast South Indian deglacial carbon release, Nat. Commun., 11, 6192, https://doi.org/10.1038/s41467-020-20034-1, 2020b.

Hain, M. P., Sigman, D. M., and Haug, G. H.: Carbon dioxide effects of Antarctic stratification, North Atlantic Intermediate Water formation, and subantarctic nutrient drawdown during the last ice age: Diagnosis and synthesis in a geochemical box model, Global Biogeochem. Cy., 24, GB4023, https://doi.org/10.1029/2010GB003790, 2010.

Hasenfratz, A. P., Jaccard, S. L., Martínez-García, A., Sigman, D. M., Hodell, D. A., Vance, D., Bernasconi, S. M., Kleiven, H. F., Haumann, F. A., and Haug, G. H.: The residence time of Southern Ocean surface waters and the 100 000-year ice age cycle, Science, 363, 1080–1084, https://doi.org/10.1126/science.aat7067, 2019.

Heaton, T. J., Köhler, P., Butzin, M., Bard, E., Reimer, R. W., Austin, W. E. N., Bronk Ramsey, C., Grootes, P. M., Hughen, K. A., Kromer, B., Reimer, P. J., Adkins, J., Burke, A., Cook, M. S., Olsen, J., and Skinner, L. C.: Marine20 – The Marine Radiocarbon Age Calibration Curve (0–55 000 cal BP), Radiocarbon, 62, 779–820, https://doi.org/10.1017/RDC.2020.68, 2020.

Henderson, G. M. and Anderson, R. F.: The U-series toolbox for paleoceanography, Rev. Mineral. Geochem., 52, 493–531, https://doi.org/10.2113/0520493, 2003.

Hoogakker, B. A. A., Elderfield, H., Schmiedl, G., McCave, I. N., and Rickaby, R. E. M.: Glacial–interglacial changes in bottom-water oxygen content on the Portuguese margin, Nat. Geosci., 8, 2–5, https://doi.org/10.1038/ngeo2317, 2015.

Horn, M. G., Robinson, R. S., Rynearson, T. A., and Sigman, D. M.: Nitrogen isotopic relationship between diatom-bound and bulk organic matter of cultured polar diatoms, Paleoceanography, 26, PA3208, https://doi.org/10.1029/2010PA002080, 2011.

Jaccard, S. L., Hayes, C. T., Hodell, D. A., Anderson, R. F., Sigman, D. M., and Haug, G. H.: Two modes of change in SO Productivity, Science, 339, 1419–1423, https://doi.org/10.1126/science.1227545, 2013.

Jaccard, S. L., Galbraith, E. D., Martínez-García, A., and Anderson, R. F.: Covariation of deep Southern Ocean oxygenation and atmospheric CO_2 through the last ice age, Nature, 530, 207–210, https://doi.org/10.1038/nature16514, 2016.

Jacobel, A. W., McManus, J. F., Anderson, R. F., and Winckler, G.: Repeated storage of respired carbon in the equatorial Pacific Ocean over the last three glacial cycles, Nat. Commun., 8, 1727, https://doi.org/10.1038/s41467-017-01938-x, 2017.

Jimenez-Espejo, F. J., Presti, M., Kuhn, G., McKay, R., Crosta, X., Escutia, C., Lucchi, R. G., Tolotti, R., Yoshimura, T., Ortega Huertas, M., Macrì, P., Caburlotto, A., and De Santis, L.: Late Pleistocene oceanographic and depositional variations along the Wilkes Land margin (East Antarctica) reconstructed with geochemical proxies in deep-sea sediments, Glob. Planet. Change, 184, 103045, https://doi.org/10.1016/j.gloplacha.2019.103045, 2020.

Jouzel, J., Masson-Delmotte, V., Cattani, O., Dreyfus, G., Falourd, S., Hoffmann, G., Minster, B., Nouet, J., Barnola, J. M., Chappellaz, J., Fischer, H., Gallet, J.C., Johnsen, S., Leuenberger, M., Loulergue, L., Luethi, D., Oerter, H., Parrenin, F., Raisbeck, G., Raynaud, D., Schilt, A., Schwander, J., Selmo, E., Souchez, R., Spahni, R., Stauffer, B., Steffensen, J. P., Stenni, B., Stocker, T. F., Tison, J. L., Werner, M., and Wolff, E. W.: Orbital and millennial antarctic climate variability over the past 800 000 years, Science, 317, 5839, 793–796, https://doi.org/10.1126/science.1141038, 2007.

Kaiser, E. A., Billups, K., and Bradtmiller, L.: A one million year record of biogenic silica in the Indian Ocean Sector of the Southern Ocean: Regional versus global forcing of primary productivity, Paleoceanogr. Paleoclimatology, 36, e2020PA004033, https://doi.org/10.1029/2020PA004033, 2021.

Klinkhammer, G. P. and Palmer, M. R.: Uranium in the oceans: Where it goes and why, Geochim. Cosmochim. Acta, 55, 1799–1806, https://doi.org/10.1016/0016-7037(91)90024-Y, 1991.

Kohfeld, K. E. and Chase, Z.: Temporal evolution of mechanisms controlling ocean carbon uptake during the last glacial cycle, Earth Planet. Sci. Lett., 472, 206–215, https://doi.org/10.1016/j.epsl.2017.05.015, 2017.

Kohfeld, K. E., Le Quéré, C., Harrison, S. P., and Anderson, R. F.: Role of marine biology in glacial-interglacial CO_2 cycles, Science, 308, 74–78, https://doi.org/10.1126/science.1105375, 2005.

Korff, L., von Dobeneck, T., Frederichs, T., Kasten, S., Kuhn, G., Gersonde, R., and Diekmann, B.: Cyclic magnetite dissolution in Pleistocene sediments of the abyssal northwest Pacific Ocean: Evidence for glacial oxygen depletion and carbon trapping, Paleoceanography, 31, 600–624, https://doi.org/10.1002/2015PA002882, 2016.

Kuhn, G.: Documentation of sediment core PS2609-1, Alfred Wegener Institute – Polarstern core repository, PANGAEA [data set], https://doi.org/10.1594/PANGAEA.115378, 2003a.

Kuhn, G.: Documentation of sediment core PS2606-6, Alfred Wegener Institute – Polarstern core repository, PANGAEA [data set], https://doi.org/10.1594/PANGAEA.115376, 2003b.

Kuhn, G.: Documentation of sediment core PS2603-3, Alfred Wegener Institute – Polarstern core repository, PANGAEA [data set], https://doi.org/10.1594/PANGAEA.115375, 2003c.

Kumar, N., Anderson, R. F., Mortlock, R. A., Froelich, P. N., Kubik, P., Dittrich-Hannen, B., and Suter, M.: Increased biological production and export in the glacial Southern Ocean, Nature, 378, 675–680, https://doi.org/10.1038/378675a0, 1995.

Lambert, F., Bigler, M., Steffensen, J. P., Hutterli, M., and Fischer, H.: Centennial mineral dust variability in high-resolution ice core data from Dome C, Antarctica, Clim. Past, 8, 609–623, https://doi.org/10.5194/cp-8-609-2012, 2012.

Lamy, F., Gersonde, R., Winckler, G., Esper, O., Jaeschke, A., Kuhn, G., Ullermann, J., Martínez-García, A., Lambert, F., and Kilian, R.: Increased dust deposition in the Pacific Southern Ocean during glacial periods, Science, 343, 403–407, https://doi.org/10.1126/science.1245424, 2014.

Langmuir, D.: Uranium solution-mineral equilibria at low temperatures with applications to sedimentary ore deposits, Geochim. Cosmochim. Acta, 42, 547–569, https://doi.org/10.1016/0016-7037(78)90001-7, 1978.

Lippold, J., Grützner, J., Winter, D., Lahaye, Y., Mangini, A., and Christi, M.: Does sedimentary $^{231}Pa\,/\,^{230}Th$ from the Bermuda Rise monitor past Atlantic Meridional Overturning Circulation?, Geophys. Res. Lett., 36, L12601, https://doi.org/10.1029/2009GL038068, 2009.

Lisiecki, L. E. and Raymo, M. E.: A Pliocene-Pleistocene stack of 57 globally distributed benthic $\delta^{18}O$ records, Paleoceanography, 20, PA1003, https://doi.org/10.1029/2004PA001071, 2005.

Lynch-Stieglitz, J., Ito, T., and Michel, E.: Antarctic density stratification and the strength of the circumpolar current during the Last Glacial Maximum, Paleoceanography, 31, 539–552, https://doi.org/10.1002/2015PA002915, 2016.

Mangini, A., Jung, M., and Laukenmann, S.: What do we learn from peaks of uranium and of manganese in deep sea sediments?, Mar. Geol., 177, 63–78, https://doi.org/10.1016/S0025-3227(01)00124-4, 2001.

Manoj, M. C. and Thamban, M.: Shifting frontal regimes and its influence on bioproductivity variations during the Late Quaternary in the Indian sector of Southern Ocean, Deep. Res. Part II, 118, 261–274, https://doi.org/10.1016/j.dsr2.2015.03.011, 2015.

Manoj, M. C., Thamban, M., Basavaiah, N., and Mohan, R.: Evidence for climatic and oceanographic controls on terrigenous sediment supply to the Indian Ocean sector of the Southern Ocean over the past 63 000 years, Geo.-Mar. Lett., 32, 251–265, https://doi.org/10.1007/s00367-011-0267-6, 2012.

Manoj, M. C., Thamban, M., Sahana, A., Mohan, R., and Mahender, K.: Provenance and temporal variability of ice rafted debris in the Indian sector of the Southern Ocean during the last 22,000 years, J. Earth Syst. Sci., 122, 491–501, https://doi.org/10.1007/s12040-013-0271-5, 2013.

Marshall, J. and Speer, K.: Closure of the meridional overturning circulation through Southern Ocean upwelling, Nat. Geosci., 5, 171–180, https://doi.org/10.1038/ngeo1391, 2012.

Martínez-García, A., Sigman, D. M., Ren, H., Anderson, R. F., Straub, M., Hodell, D. A., Jaccard, S. L., Eglinton, T. I., and Haug, G. H.: Iron fertilization of the subantarctic ocean during the last ice age, Science, 343, 1347–1350, https://doi.org/10.1126/science.1246848, 2014.

Matsumoto, K., Sarmiento, J. L., and Brzezinski, M. A.: Silicic acid leakage from the Southern Ocean: A possible explanation for glacial atmospheric pCO_2, Global Biogeochem. Cy., 16, 1031, https://doi.org/10.1029/2001GB001442, 2002.

Meyerink, S. W., Ellwood, M. J., Maher, W. A., Dean Price, G., and Strzepek, R. F.: Effects of iron limitation on silicon uptake kinetics and elemental stoichiometry in two Southern Ocean diatoms, Eucampia antarctica and Proboscia inermis, and the temperate diatom Thalassiosira pseudonana, Limnol. Oceanogr., 62, 2445–2462, https://doi.org/10.1002/lno.10578, 2017.

Morford, J. L. and Emerson, S.: The geochemistry of redox sensitive trace metals in sediments, Geochim. Cosmochim. Acta, 63, 1735–1750, https://doi.org/10.1016/S0016-7037(99)00126-X, 1999.

Müller, P. J. and Schneider, R.: An automated leaching method for the determination of opal in sediments and particulate matter, Deep. Res. Part I, 40, 425–444, https://doi.org/10.1016/0967-0637(93)90140-X, 1993.

Nair, A., Mohan, R., Crosta, X., Manoj, M. C., Thamban, M., and Marieu, V.: Southern Ocean sea ice and frontal changes during the Late Quaternary and their linkages to Asian summer monsoon, Quaternary Sci. Rev., 213, 93–104, https://doi.org/10.1016/j.quascirev.2019.04.007, 2019.

Nameroff, T. J., Balistrieri, L. S., and Murray, J. W.: Suboxic trace metal geochemistry in the eastern tropical North Pacific, Geochim. Cosmochim. Acta, 66, 1139–1158, https://doi.org/10.1016/S0016-7037(01)00843-2, 2002.

Nelson, D. M., Anderson, R. F., Barber, R. T., Brzezinski, M. A., Buesseler, K. O., Chase, Z., Collier, R. W., Dickson, M. L., François, R., Hiscock, M. R., Honjo, S., Marra, J., Martin, W. R., Sambrotto, R. N., Sayles, F. L., and Sigmon, D. E.: Vertical budgets for organic carbon and biogenic silica in the Pacific sector of the Southern Ocean, 1996–1998, Deep. Res. Part II, 49, 1645–1674, https://doi.org/10.1016/S0967-0645(02)00005-X, 2002.

Oiwane, H., Ikehara, M., Suganuma, Y., Miura, H., Nakamura, Y., Sato, T., Nogi, Y., Yamane, M., and Yokoyama, Y.: Sediment waves on the Conrad Rise, Southern Indian Ocean: Implications for the migration history of the Antarctic Circumpolar Current, Mar. Geol., 348, 27–36, https://doi.org/10.1016/j.margeo.2013.10.008, 2014.

Oliver, K. I. C., Hoogakker, B. A. A., Crowhurst, S., Henderson, G. M., Rickaby, R. E. M., Edwards, N. R., and Elderfield, H.: A synthesis of marine sediment core δ13C data over the last 150 000 years, Clim. Past, 6, 645–673, https://doi.org/10.5194/cp-6-645-2010, 2010.

Orsi, H., Whitworth, T., and Nowlin Jr., W. D.: On the meridional extent and fronts of the Antarctic Circumpolar Current, Deep. Res. Part I, 42, 641–673, https://doi.org/10.1016/0967-0637(95)00021-W, 1995.

Pichat, S., Sims, K. W. W., François, R., McManus, J. F., Leger, S. B., and Albarède, F.: Lower export production during glacial periods in the equatorial Pacific derived from $(^{231}Pa\,/\,^{230}Th)_{xs,0}$ measurements in deep-sea sediments, Paleoceanography, 19, PA4023, https://doi.org/10.1029/2003PA000994, 2004.

Pichevin, L. E., Ganeshram, R. S., Geibert, W., Thunell, R., and Hinton, R.: Silica burial enhanced by iron limitation in oceanic upwelling margins, Nat. Geosci., 7, 541–546, https://doi.org/10.1038/ngeo2181, 2014.

Pondaven, P., Ragueneau, O., Tréguer, P., Hauvespre, A., Dezileau, L., and Reyss, J. L.: Resolving the 'opal paradox' in the Southern Ocean, Nature, 405, 168–172, https://doi.org/10.1038/35012046, 2000.

Rae, J. W. B., Burke, A., Robinson, L., Adkins, J. F., Chen, T., Cole, C., Greenop, R., Li, T., Littley, E. F. M., Nita, D. C., Steward, J. A., and Taylor, B. J.: CO_2 storage and release in the deep Southern Ocean on millennial to centennial timescales, Nature, 562, 569–573, https://doi.org/10.1038/s41586-018-0614-0, 2018.

Ragueneau, O., Tréguer, P., Leynaert, A., Anderson, R. F., Brzezinski, M. A., DeMaster, D. J., Dugdale, R. C., Dymond, J., Fischer, G., François, R., Heinze, C., Maier-Reimer, E., Martin-Jézéquel, V., Nelson, D. M., and Quéguiner, B.: A review of the Si cycle in the modern ocean: Recent progress and missing gaps in the application of biogenic opal as a paleoproductivity proxy, Glob. Planet. Change, 26, 317–365, https://doi.org/10.1016/S0921-8181(00)00052-7, 2000.

Reimer, P. J., Bard, E., Bayliss, A., Beck, J. W., Blackwell, P. G., Bronk Ramsey, C., Buck, C. E., Cheng, H., Edwards, R. L., Friedrich, M., Grootes, P. M., Guilderson, T. P., Haflidason, H., Hajdas, I., Hatté, C., Heaton, T. J., Hoffmann, D. L., Hogg, A. G., Hughen, K., A., Kaiser, K. F., Kromer, B., Manning, S. W., Niu, M., Reimer, R. W., Richards, D. A., Scott, E. M., Southon, J. R., Staff, R. A., Turney, C. S. M., and van der Plicht, J.: IntCal13 and Marine13 Radiocarbon Age Calibration Curves 0–50 000 Years cal BP, Radiocarbon, 55, 1869–1887, https://doi.org/10.2458/azu_js_rc.55.16947, 2013.

Ronge, T. A., Prange, M., Mollenhauer, G., Ellinghausen, M., Kuhn, G., and Tiedemann, R.: Radiocarbon Evidence for the Contribution of the Southern Indian Ocean to the Evolution of Atmospheric CO_2 Over the Last 32 000 Years, Paleoceanogr. Paleoclimatol., 35, e2019PA003733, https://doi.org/10.1029/2019PA003733, 2020.

Sakamoto, T., Kuroki, K., Sugawara, T., Aoike, K., Iijima, K., and Sugisaki, S.: Non-Destructive X-Ray Fluorescence (XRF) Core-Imaging Scanner, TATSCAN-F2, Sci. Dril., 2, 37–39, https://doi.org/10.5194/sd-2-37-2006, 2006.

Sarnthein, M., Schneider, B., and Grootes, P. M.: Peak glacial 14C ventilation ages suggest major draw-down of carbon into the abyssal ocean, Clim. Past, 9, 2595–2614, https://doi.org/10.5194/cp-9-2595-2013, 2013.

Sayles, F. L., Martin, W. R., Chase, Z., and Anderson, R. F.: Benthic remineralization and burial of biogenic SiO_2, $CaCO_3$, organic carbon, and detrital material in the Southern Ocean along a transect at 170° West, Deep. Res. Part II, 48, 19–20, 4323–4383, https://doi.org/10.1016/S0967-0645(01)00091-1, 2001.

Schlitzer, R.: Ocean Data View, Ocean Data View, http://odv.awi.de (last access: 13 March 2019), 2018.

Sigman, D. M. and Boyle, E. A.: Glacial/interglacial variations in atmospheric carbon dioxide, Nature, 407, 859–869, https://doi.org/10.1038/35038000, 2000.

Sigman, D. M., Hain, M. P., and Haug, G. H.: The polar ocean and glacial cycles in atmospheric CO_2 concentration, Nature, 466, 47–55, https://doi.org/10.1038/nature09149, 2010.

Sigman, D. M., Fripiat, F., Studer, A. S., Kemeny, P. C., Martínez-García, A., Hain, M. P., Ai, X., Wang, X., Ren, H., and Haug, G. H.: The Southern Ocean during the ice ages: A review of the Antarctic surface isolation hypothesis, with comparison to the North Pacific, Quaternay Sci. Rev., 254, 106732, https://doi.org/10.1016/j.quascirev.2020.106732, 2021.

Skinner, L. C.: Glacial-interglacial atmospheric CO_2 change: a possible "standing volume" effect on deep-ocean carbon sequestration, Clim. Past, 5, 537–550, https://doi.org/10.5194/cp-5-537-2009, 2009.

Skinner, L. C., Fallon, S., Waelbroeck, C., Michel, E., and Barker, S.: Ventilation of the Deep Southern Ocean and Deglacial CO_2 Rise, Science, 328, 1147–1151, https://doi.org/10.1126/science.1183627, 2010.

Skinner, L. C., Primeau, F., Freeman, E., de la Fuente, M., Goodwin, P. A., Gottschalk, J., Huang, E., McCave, I. N., Noble, T. L., and Scrivner, A. E.: Radiocarbon constraints on the glacial ocean circulation and its impact on atmospheric CO_2, Nat. Commun., 8, 16010, https://doi.org/10.1038/ncomms16010, 2017.

Sruthi, K. V., Thamban, M., Manoj, M. C., and Laluraj, C. M.: Association of trace elements with various geochemical phases in the Indian sector of Southern Ocean during past 22 000 years and its palaeoceanographic implications, Curr. Sci., 103, 803–809, 2012.

Stein, K., Timmermann, A., Young Kwon, E., and Friedrich, T.: Timing and magnitude of Southern Ocean sea ice/carbon cycle feedbacks, P. Natl. Acad. Sci. USA, 117, 9, https://doi.org/10.1073/pnas.1908670117, 2020.

Studer, A. S., Sigman, D. M., Martínez-García, A., Benz, V., Winckler, G., Kuhn, G., Esper, O., Lamy, F., Jaccard, S. L., Wacker, L., Oleynik, S., Gersonde, R., and Haug, G. H.: Antarctic Zone nutrient conditions during the last two glacial cycles, Paleoceanography, 30, 845–862, https://doi.org/10.1002/2014PA002745, 2015.

Stuiver, M. and Reimer, P. J.: Extended ^{14}C database and revised CALIB radiocarbon calibration program, Radiocarbon, 35, 215–230, https://doi.org/10.1017/S0033822200013904, 1993.

Stuiver, M., Reimer, P. J., Bard, E., Beck, J. W., Burr, G. S., Hughen, K. A., Kromer, B., McCormac, G., van der Plicht, J., and Spurk, M.: INTCAL98 radiocarbon age calibration, 24 000–0 cal BP, Radiocarbon, 40, 1041–1083, https://doi.org/10.1017/S0033822200019123, 1998.

Tagliabue, A., Sallée, J.-B., Bowie, A. R., Lévy, M., Swart, S., and Boyd, P. W.: Surface-water iron supplies in the Southern Ocean sustained by deep winter mixing, Nat. Geosci., 7, 314–320, https://doi.org/10.1038/ngeo2101, 2014.

Talley, L. D.: Closure of the global overturning circulation through the Indian, Pacific, and Southern Oceans: Schematics and transports, Oceanography, 26, 80–97, https://doi.org/10.5670/oceanog.2013.07, 2013.

Thöle, L. M., Amsler, H. E., Moretti, S., Auderset, A., Gilgannon, J., Lippold, J., Vogel, H., Crosta, X., Mazaud, A., Michel, E., Martínez-García, A., and Jaccard, S. L.: Glacial-interglacial dust and export production records from the Southern Indian Ocean, Earth Planet. Sci. Lett., 525, 115716, https://doi.org/10.1016/j.epsl.2019.115716, 2019.

Thomson, J., Wallace, H. E., Colley, S., and Toole, J.: Authigenic uranium in Atlantic sediments of the last glacial stage – a diagenetic phenomenon, Earth Planet. Sci. Lett., 98, 222–232, https://doi.org/10.1016/0012-821x(90)90061-2, 1990.

Toggweiler, J. R.: Variation of atmospheric CO_2 by ventilation of the ocean's deepest water, Paleoceanography, 14, 571–588, https://doi.org/10.1029/1999PA900033, 1999.

Toggweiler, J. R., Russell, J. L., and Carson, S. R.: Midlatitude westerlies, atmospheric CO_2, and climate change during the ice ages, Paleoceanography, 21, PA2005, https://doi.org/10.1029/2005PA001154, 2006.

Tribovillard, N., Algeo, T. J., Lyons, T., and Riboulleau, A.: Trace metals as paleoredox and paleoproductivity proxies: An update, Chem. Geol., 232, 12–32, https://doi.org/10.1016/j.chemgeo.2006.02.012, 2006.

Vogel, H., Meyer-Jacob, C., Thöle, L. M., Lippold, J. A., and Jaccard, S. L.: Quantification of biogenic silica by means of Fourier transform infrared spectroscopy (FTIRS) in marine sediments, Limnol. Oceanogr. Methods, 14, 828–838, https://doi.org/10.1002/lom3.10129, 2016.

Watson, A. J. and Naveira Garabato, A. C.: The role of Southern Ocean mixing and upwelling in glacial-interglacial atmospheric CO_2 change, Tellus B, 58, 73–87, https://doi.org/10.1111/j.1600-0889.2005.00167.x, 2006.

Watson, A. J., Vallis, G. K., and Nikurashin, M.: Southern Ocean buoyancy forcing of ocean ventilation and glacial atmospheric CO_2, Nat. Geosci., 8, 861–864, https://doi.org/10.1038/ngeo2538, 2015.

Weber, M. E., Kuhn, G., Sprenk, D., Rolf, C., Ohlwein, C., and Ricken, W.: Dust transport from Patagonia to Antarctica – A new stratigraphic approach from the Scotia Sea and its implications for the last glacial cycle, Quaternary Sci. Rev., 36, 177–188, https://doi.org/10.1016/j.quascirev.2012.01.016, 2012.

Weber, M. E., Clark, P. U., Kuhn, G., Timmermann, A., Sprenk, D., Gladstone, R., Zhang, X., Lohmann, G., Menviel, L., Chikamoto, M. O., Friedrich, T., and Ohlwein, C.: Millennial-scale variability in Antarctic ice-sheet discharge during the last deglaciation, Nature, 510, 134–138, https://doi.org/10.1038/nature13397, 2014.

Wilson, D. J., Piotrowski, A. M., Galy, A., and Banakar, V. K.: Interhemispheric controls on deep ocean circulation and carbon chemistry during the last two glacial cycles, Paleoceanography, 30, 621–641, https://doi.org/10.1002/2014PA002707, 2015.

Wolff, E. W., Barbante, C., Becagli, S., Bigler, M., Boutron, C. F., Castellano, E., de Angelis, M., Federer, U., Fischer, H., Fundel, F., Hansson, M., Hutterli, M., Jonsell, U., Karlin, T., Kaufmann, P., Lambert, F., Littot, G. C., Mulvaney, R., Röthlisberger, R., Ruth, U., Severi, M., Siggaard-Andersen, M. L., Sime, L. C., Steffensen, J. P., Stocker, T. F., Traversi, R., Twarloh, B., Udisti, R., Wagenbach, D., and Wegner, A.: Changes in environment over the last 800 000 years from chemical analysis of the EPICA Dome C ice core, Quaternary Sci. Rev., 29, 285–295, https://doi.org/10.1016/j.quascirev.2009.06.013, 2010.

Wu, S., Lembke-Jene, L., Lamy, F., Arz, H. W., Nowaczyk, N., Xiao, W., Zhang, X., Hass, H. C., Titschack, J., Zheng, X., Liu, J., Dumm, L., Diekmann, B., Nürnberg, D., Tiedemann, R., and Kuhn, G: Orbital- and millennial-scale Antarctic Circumpolar Current variability in Drake Passage over the past 140 000 years, Nat. Commun., 12, 3948, https://doi.org/10.1038/s41467-021-24264-9, 2021.

Xiao, W., Esper, O., and Gersonde, R.: Last Glacial – Holocene climate variability in the Atlantic sector of the Southern Ocean, Quaternary Sci. Rev., 135, 115–137, https://doi.org/10.1016/j.quascirev.2016.01.023, 2016.

Yu, J., Menviel, L., Jin, Z. D., Thornalley, D. J. R., Barker, S., Marino, G., Rohling, E. J., Cai, Y., Zhang, F., Wang, X., Dai, Y., Chen, P., and Broecker, W. S.: Sequestration of carbon in the deep Atlantic during the last glaciation, Nat. Geosci., 9, 319–324, https://doi.org/10.1038/ngeo2657, 2016.

Zielinski, U. and Gersonde, R.: Plio-Pleistocene diatom biostratigraphy from ODP Leg 177, Atlantic sector of the Southern Ocean, Mar. Micropaleontol., 45, 225–268, https://doi.org/10.1016/S0377-8398(02)00031-2, 2002.